7-20-2008

A Measurement of the Rate of Type Ia Supernovae at Redshift z ≈ 0.1 from the First Season of the SDSS-II Supernova Survey

Benjamin Dilday
University of Chicago

Richard Kessler
University of Chicago

Joshua Frieman
University of Chicago

Michael W. Richmond
Rochester Institute of Technology

et al.

Recommended Citation
Benjamin Dilday et al 2008 ApJ 682 262 https://doi.org/10.1086/587733

A Measurement of the Rate of type Ia Supernovae at Redshift $z \approx 0.1$ from the First Season of the SDSS-II Supernova Survey

bdilday@uchicago.edu

Benjamin Dilday,[1,2] Richard Kessler,[2,3] Joshua A. Frieman,[2,4,5] Jon Holtzman,[6] John Marriner,[5] Gajus Miknaitis,[5] Robert C. Nichol,[7] Roger Romani,[8] Masao Sako,[8,9] Bruce Bassett,[10,11] Andrew Becker,[12] David Cinabro,[13] Fritz DeJongh,[5] Darren L. Depoy,[14] Mamoru Doi,[15] Peter M. Garnavich,[16] Craig J. Hogan,[12] Saurabh Jha,[8,17] Kohki Konishi,[18] Hubert Lampeitl,[7,19] Jennifer L. Marshall,[14] David McGinnis,[5] Jose Luis Prieto,[14] Adam G. Riess,[19,20] Michael W. Richmond,[21] Donald P. Schneider,[22] Mathew Smith,[7] Naohiro Takanashi,[15] Kouichi Tokita,[15] Kurt van der Heyden,[11,23] Naoki Yasuda,[18] Chen Zheng,[8] John Barentine,[24,25] Howard Brewington,[25] Changsu Choi,[26] Arlin Crotts,[27] Jack Dembicky,[25] Michael Harvanek,[25,28] Myunshin Im,[26] William Ketzeback,[25] Scott J. Kleinman,[25,29] Jurek Krzesiński,[25,30] Daniel C. Long,[25] Elena Malanushenko,[25] Viktor Malanushenko,[25] Russet J. McMillan,[25] Atsuko Nitta,[25,31] Kaike Pan,[25] Gabrelle Saurage,[25] Stephanie A. Snedden,[25] Shannon Watters,[25] J. Craig Wheeler,[24] and Donald York[3,4]

[1] Department of Physics, University of Chicago, Chicago, IL 60637.

[2] Kavli Institute for Cosmological Physics, The University of Chicago, 5640 South Ellis Avenue Chicago, IL 60637.

[3] Enrico Fermi Institute, University of Chicago, 5640 South Ellis Avenue, Chicago, IL 60637.

[4] Department of Astronomy and Astrophysics, The University of Chicago, 5640 South Ellis Avenue, Chicago, IL 60637.

[5] Center for Particle Astrophysics, Fermi National Accelerator Laboratory, P.O. Box 500, Batavia, IL 60510.

[6] Department of Astronomy, MSC 4500, New Mexico State University, P.O. Box 30001, Las Cruces, NM 88003.

[7] Institute of Cosmology and Gravitation, Mercantile House, Hampshire Terrace, University of Portsmouth, Portsmouth PO1 2EG, UK.

[8] Kavli Institute for Particle Astrophysics & Cosmology, Stanford University, Stanford, CA 94305-4060.

[9] Department of Physics and Astronomy, University of Pennsylvania, 203 South 33rd Street, Philadelphia, PA 19104.

[10] Department of Mathematics and Applied Mathematics, University of Cape Town, Rondebosch 7701, South Africa.

[11] South African Astronomical Observatory, P.O. Box 9, Observatory 7935, South Africa.

[12] Department of Astronomy, University of Washington, Box 351580, Seattle, WA 98195.

[13] Department of Physics, Wayne State University, Detroit, MI 48202.

[14] Department of Astronomy, Ohio State University, 140 West 18th Avenue, Columbus, OH 43210-1173.

[15] Institute of Astronomy, Graduate School of Science, University of Tokyo 2-21-1, Osawa, Mitaka, Tokyo 181-0015, Japan.

[16] University of Notre Dame, 225 Nieuwland Science, Notre Dame, IN 46556-5670.

[17] Department of Physics and Astronomy, Rutgers University, 136 Frelinghuysen Road, Piscataway, NJ 08854.

[18] Institute for Cosmic Ray Research, University of Tokyo, 5-1-5, Kashiwanoha, Kashiwa, Chiba, 277-8582, Japan.

[19] Space Telescope Science Institute, 3700 San Martin Drive, Baltimore, MD 21218.

[20] Department of Physics and Astronomy, Johns Hopkins University, 3400 North Charles Street, Baltimore, MD 21218.

[21] Physics Department, Rochester Institute of Technology, 85 Lomb Memorial Drive, Rochester, NY 14623-5603.

[22] Department of Astronomy and Astrophysics, The Pennsylvania State University, 525 Davey Laboratory,

ABSTRACT

We present a measurement of the rate of type Ia supernovae (SNe Ia) from the first of three seasons of data from the SDSS-II Supernova Survey. For this measurement, we include 17 SNe Ia at redshift $z \leq 0.12$. Assuming a flat cosmology with $\Omega_m = 0.3 = 1 - \Omega_\Lambda$, we find a volumetric SN Ia rate of $[2.93^{+0.17}_{-0.04}(\text{systematic})^{+0.90}_{-0.71}(\text{statistical})] \times 10^{-5}$ SNe Mpc^{-3} h^3_{70} year^{-1}, at a volume-weighted mean redshift of 0.09. This result is consistent with previous measurements of the SN Ia rate in a similar redshift range. The systematic errors are well controlled, resulting in the most precise measurement of the SN Ia rate in this redshift range. We use a maximum likelihood method to fit SN rate models to the SDSS-II Supernova Survey data in combination with other rate measurements, thereby constraining models for the redshift-evolution of the SN Ia rate. Fitting the combined data to a simple power-law evolution of the volumetric SN Ia rate, $r_V \propto (1+z)^\beta$, we obtain a value of $\beta = 1.5 \pm 0.6$, i.e. the SN Ia rate is determined to be an increasing function of redshift at the $\sim 2.5\sigma$ level. Fitting the results to a model in which the volumetric SN rate, $r_V = A\rho(t) + B\dot{\rho}(t)$, where $\rho(t)$ is the stellar mass density and $\dot{\rho}(t)$ is the star formation rate, we find $A = (2.8 \pm 1.2) \times 10^{-14}$ SNe M$_\odot^{-1}$ year^{-1}, $B = (9.3^{+3.4}_{-3.1}) \times 10^{-4}$ SNe M$_\odot^{-1}$.

Subject headings: supernovae: general

University Park, PA 16802.

[22] Department of Physics and Astronomy, University of Pennsylvania, 203 South 33rd Street, Philadelphia, PA 19104.

[23] Department of Astronomy, University of Cape Town, South Africa.

[24] Department of Astronomy, McDonald Observatory, University of Texas, Austin, TX 78712

[25] Apache Point Observatory, P.O. Box 59, Sunspot, NM 88349.

[26] Department of Astronomy, Seoul National University, Seoul, South Korea.

[27] Department of Astronomy, Columbia University, New York, NY 10027.

[28] Lowell Observatory, 1400 Mars Hill Rd., Flagstaff, AZ 86001

[29] Subaru Telescope, 650 N. A'Ohoku Place, Hilo, HI 96720

[30] Obserwatorium Astronomiczne na Suhorze, Akademia Pedagogicazna w Krakowie, ulica Podchorążych 2, PL-30-084 Kraków, Poland.

[31] Gemini Observatory, 670 North A'ohuoku Place, Hilo, HI 96720.

1. Introduction

Type Ia supernovae (SNe Ia) have gained increasing attention from astronomers, primarily due to their remarkable utility as cosmological distance indicators. There is now broad consensus that a type Ia supernova is the thermonuclear explosion of a Carbon-Oxygen white dwarf star that accretes mass from a binary companion until it reaches the Chandrasekhar mass limit (e.g. Branch et al. (1995)). However, much remains to be learned about the physics of SNe Ia, and there is active debate about both the nature of the progenitor systems and the details of the explosion mechanism. For example, the binary companion may be a main-sequence star, a giant or sub-giant, or a second white dwarf. The type of the companion star determines in part the predicted time delay between the formation of the binary system and the SN event (Greggio 2005). The time delay can be constrained observationally by comparing the SN Ia rate as a function of redshift to the star formation history (SFH) (Strolger et al. 2004; Cappellaro et al. 2007).

The insight into the nature of the progenitor systems that SN Ia rate measurements provide can also potentially strengthen the utility of SNe Ia as cosmological distance indicators. Although the strong correlation between SN Ia peak luminosity and light curve decline rate was found purely empirically (Pskovskii 1977; Phillips 1993), the physics underlying this relation has been extensively studied (Höflich et al. 1995, 1996; Kasen & Woosley 2007). There is hope that improved physical understanding and modeling of SN Ia explosions, coupled with larger high-quality observational data sets, will lead to improved distance estimates from SNe Ia. As part of this program, deeper understanding of the nature of the progenitor systems can help narrow the range of initial conditions that need to be explored in carrying out the costly simulations of SN Ia explosions that in principle predict their photometric and spectroscopic properties.

Measurement of the SN Ia rate may also have a more direct impact on the determination of systematic errors in SN Ia distance estimates. Mannucci et al. (2006); Scannapieco & Bildsten (2005); Neill et al. (2006) and Sullivan et al. (2006) have argued that a two-component model of the SN Ia rate, in which a prompt SN component follows the star formation rate and a second component follows the total stellar mass, is strongly favored over a single SN Ia channel. In this picture, since the cosmological star formation rate increases sharply with lookback time, the prompt component is expected to dominate the total SN Ia rate at high redshift. Mannucci et al. (2006) and Howell et al. (2007) pointed out that this evolution with redshift can be a potential source of systematic error in SN Ia distance estimates, if the two populations have different properties.

In order to test such a model for the evolution of the SN Ia rate, improved measurements of the rate as a function of redshift and of host galaxy properties are needed. The Supernova

Legacy Survey (SNLS) has recently presented the most precise measurement of the SN Ia rate at high redshift ($z \sim 0.5$) based on 73 SNe Ia (Neill et al. 2006; Sullivan et al. 2006). At low redshifts ($z \sim 0.1$), SN Ia rate measurements (Cappellaro et al. 1999; Hardin et al. 2000; Madgwick et al. 2003; Blanc et al. 2004) have suffered from small sample sizes and also from systematic errors associated with heterogeneous samples (Cappellaro et al. 1999) and with selection biases due to the targeting of known, relatively luminous galaxies (Hardin et al. 2000; Blanc et al. 2004). The low-redshift measurement of Madgwick et al. (2003), based on SNe discovered fortuitously in SDSS galaxy spectra, is affected by different systematic uncertainties than traditional photometric searches, e.g., due to the finite aperture of the SDSS spectroscopic fibers.

In this paper, we present a new measurement of the SN Ia rate at low redshift, based upon the first season of data from the SDSS-II Supernova Survey. The SDSS-II Supernova Survey (Frieman et al. 2008) offers several advantages for this measurement. It covers a larger spatial volume than previous SN surveys, a result of the combination of intermediate-scale (2.5-m) telescope aperture, wide field of view (3 square degrees), modest effective sidereal exposure time (54 sec), and use of drift-scanning to efficiently cover a large sky area ($\sim$ 300 square degrees). The SDSS-II Supernova Survey is a rolling search, with new SNe discovered simultaneously with the follow-up of previously discovered SNe. Unlike SN searches that target known galaxies, the SDSS-II Supernova Survey is not biased against finding SNe in low-luminosity host galaxies. Well-calibrated photometry in the SDSS *ugriz* passbands (Fukugita et al. 1996), with a typical interval between observations of four days, yields well-sampled, multi-band light curves that enable photometric typing of SNe with high confidence. Moreover, rapid on-mountain photometric reduction and image processing coupled with an extensive spectroscopic follow-up program enable spectroscopic confirmation of a very high fraction of the low-redshift SN Ia candidates.

The SDSS-II Supernova Survey was carried out over three three-month seasons, during Sept.-Nov. 2005-7. The results presented here are based on the Fall 2005 season. The SDSS-II Supernova Survey measures light curves for SNe Ia to redshift $z \simeq 0.4$, with a median redshift of $\langle z \rangle = 0.22$ for spectroscopically confirmed SNe Ia. However, in this first paper we limit the analysis to low redshift, $z \leq 0.12$, since our spectroscopic follow-up is essentially complete over this redshift range, and the uncertainty due to spectroscopically unobserved (and untyped) SNe is therefore negligible. In presenting a SN Ia rate measurement, one must decide whether to include peculiar SNe Ia, i.e., events that are photometrically and/or spectroscopically unusual, since it is not clear that they are members of the same population as the "normal" SNe Ia. Formerly, the peculiar designation included events such as 1991T and 1991bg, which are highly overluminous and underluminous events, respectively. However, since these SNe appear to follow the standard peak-luminosity/decline-rate relation, they are

now generally considered extreme members of the normal SN Ia population (Nugent et al. 1995). Other events, such as 2002ic (Hamuy et al. 2003) and 2002cx (Li et al. 2003), exhibit more pronounced peculiarities and do not fit the luminosity-decline relation. The first season of the SDSS-II Supernova Survey included two such truly peculiar events at low redshift, 2005hk (Phillips et al. 2007) and 2005gj (Prieto et al. 2007; Aldering et al. 2006). Although these peculiar events may arise from the same evolutionary path as normal SNe Ia, which would argue for including them in a SN Ia rate measurement, we have chosen to include only SNe with light curves that obey the standard brightness-decline relation. More specifically, we include in our rate measurement sample only SNe with light curves that are well described by the MLCS2k2 SN Ia light curve model (Riess et al. 1996; Jha et al. 2007), see §3.1. Regardless of the physical arguments surrounding peculiar events, we exclude them from this analysis primarily because we do not yet have a robust determination of our efficiency for detecting them.

The rest of the paper is organized as follows. In §2 we provide a brief outline of the survey observing strategy and operations as they relate to the rate determination. In §3 we define selection criteria and present the sample of SNe Ia used in this measurement, based on spectroscopic and photometric measurements. In §4 we present estimates of the detection efficiency for low-redshift SNe Ia, based on artificial SNe inserted into the survey images and on Monte Carlo simulations. We present our measurement of the SN Ia rate and discuss the SN Ia rate as a function of host galaxy type in §5. In §6 we compare our result to other SN Ia rate measurements and combine rate measurements to fit semi-empirical models of rate evolution.

2. SDSS-II Supernova Survey Overview

Here we briefly describe the SDSS-II Supernova Survey, highlighting the features that are most relevant to a rate measurement. The survey is described in more detail in Frieman et al. (2008) and in Sako et al. (2008). A technical summary of the SDSS is given by York et al. (2000), and further details can be found in Hogg et al. (2001); Ivezić et al. (2004); Lupton et al. (1999); Smith et al. (2002); Tucker et al. (2006).

2.1. Imaging

The SDSS-II Supernova Survey is carried out on the 2.5m telescope (Gunn et al. 2006) at Apache Point Observatory (APO), using a wide-field CCD camera (Gunn et al. 1998)

operating in time-delay-and-integrate (TDI, or drift scan) mode. Observations are obtained nearly simultaneously in the SDSS *ugriz* filter bands (Fukugita et al. 1996).

The SDSS-II Supernova Survey covers a region, designated stripe 82, centered on the celestial equator in the Southern Galactic hemisphere, bounded by $-60^\circ < \alpha_{J2000} < 60^\circ$, and $-1.258^\circ < \delta_{J2000} < 1.258^\circ$. Stripe 82 has been imaged multiple times in photometric conditions by the SDSS-I survey; co-added images from those runs provide deep template images and veto catalogs of variable objects for the SDSS-II Supernova Survey transient search. Due to gaps between the CCD columns on the camera, each stripe is divided into northern (N) and southern (S) *strips*; the SDSS-II Supernova Survey alternates between the N and S strips on subsequent nights. Each strip encompasses ~ 162 square degrees of sky, with a small overlap between them, so that the survey covers ~ 300 square degrees. On average each part of the survey region was observed once every four nights during the 2005 season. Figure 1 shows the sky coverage versus survey time, along with a representative SN Ia light curve.

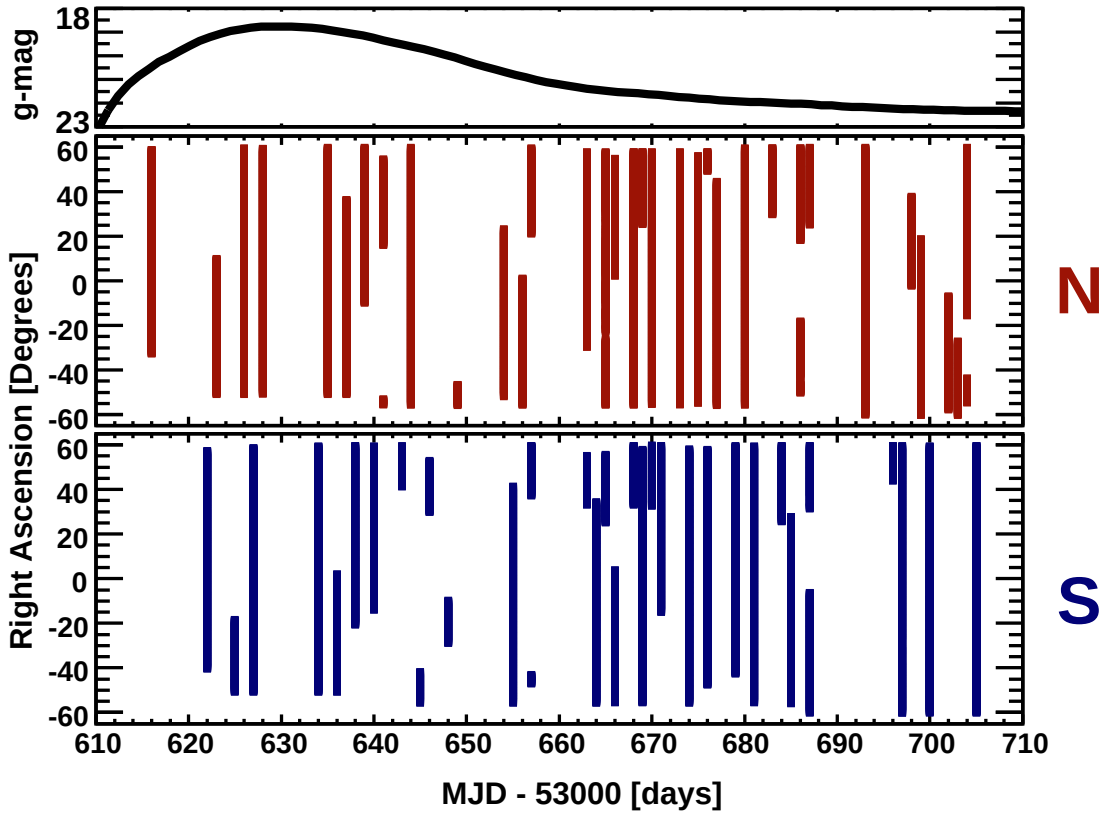

Fig. 1.— Right ascension range covered by SDSS-II Supernova Survey imaging runs vs. epoch. The panels labelled N & S denote the Northern and Southern strips of stripe 82. The regions $\alpha_{J2000} < -51°$ and $\alpha_{J2000} > 57°$ are not covered early in the season, and these regions are suppressed from the rate measurement. The top panel shows an example unextincted g-band light curve for a SN Ia at a redshift of 0.12, based on the MLCS2k2 model.

2.2. Supernova Search Pipeline

There are five main components to the supernova search pipeline: photometric reduction, image subtraction, automated object selection, visual inspection, and light curve fitting for spectroscopic target selection. We describe them briefly in turn. For a full night of imaging data, the entire pipeline runs in approximately 20 hours, sufficient for keeping up with the data flow and for rapid spectroscopic targeting.

In the first stage of the search pipeline, the imaging data is acquired from the camera and processed through the the SDSS photometric reduction pipeline, known as `PHOTO` (Lupton et al. 2001). `PHOTO` produces "corrected" images that are astrometrically calibrated (Pier et al. 2003) and provides a local estimate of the point spread function (PSF). In the second stage, images are processed through the difference imaging pipeline. To run the search pipeline to completion in less than a day with the available on-mountain computing resources, only the corrected *gri* images are processed beyond the first stage. The search image is astrometrically and photometrically registered to the template image, and the template image is convolved with a kernel chosen to minimize subtraction residuals (Alard & Lupton 1998). A difference image is then obtained by subtracting the convolved template image from the survey image. Peaks are detected in the difference image using the `DoPHOT` photometry and object detection package (Schechter et al. 1993). The signal-to-noise threshold for object detection is at ~ 3.5, corresponding in typical conditions to $g \sim 23.2$, $r \sim 22.8$, and $i \sim 22.5$. The typical magnitudes at signal-to-noise of 10 for point-like objects are $g \sim 21.8$, $r \sim 21.5$, and $i \sim 21.2$.

The third stage of the SN search pipeline comprises a sequence of automated filtering operations that select events of potential interest from among those detected in the difference images. We require a close positional match in at least two of the *gri* images, which removes cosmic rays, single-band spurious noise fluctuations, and a large fraction of asteroids and other rapidly moving objects detected by the survey. All detections that satisfy these criteria are entered into a `MySQL` database and are referred to as *objects*. To reject active galactic nuclei (AGN) and variable stars, we veto any detection occurring at the position of a previously cataloged variable, using observations of stripe 82 from several previous years. The area corresponding to previously cataloged variable objects represents $\sim 1\%$ of the total survey area.

In addition to SNe, the database of detected objects includes a variety of physical and non-physical transients. Physical sources include slow-moving asteroids that were not rejected by the moving object veto, AGN and variable stars not already cataloged, and high proper-motion stars. Non-physical sources include improperly masked diffraction spikes from bright stars and artifacts of imperfect image registration. To remove non-physical sources,

cut-out images of all objects that remain after the automated filtering are visually inspected and classified in the fourth stage of the search pipeline. Objects visually classified as consistent with a possible SN event are flagged for further analysis and are denoted *candidates*. Subsequent object detections in difference images at the same position are automatically associated with the same candidate.

In the fifth and final stage of processing for the SN search, the *gri* light curve for each SN candidate is fit to models of type-Ia, type-Ib/c and type-II SNe. The non-Ia SN models consist of template light curves constructed from photometric measurements of individual SNe provided by the SUSPECT database[1], coupled with the corresponding SN spectral model provided by Nugent et al. (2002). For the SN Ia model, a stretch and a wavelength-dependent scale factor is applied to a fiducial bolometric light curve in a way designed to reproduce the Δm_{15} parameterization of the peak-luminosity/decline-rate relation (Hamuy et al. 1996). The time of maximum, Δm_{15}, redshift, and extinction parameter A_V (magnitudes of extinction in the V-band) are fit parameters that are searched on a grid for the set of values that produce the minimum value of the χ^2 statistic. For some candidates, we additionally carry out difference imaging in the u and z passbands in order to better distinguish Type II and Type Ia SNe that tend to have a significantly different $u-g$ color at early epochs. To further constrain the early light curve shape, we carry out forced-positional photometry on difference images at the position of the candidate in pre-discovery images. The relative goodness of fit of candidate *gri* light curves to SNe Ia and core-collapse SNe models is used as a factor in prioritizing spectroscopic follow-up. In particular, all SN Ia candidates found before peak and with estimated current r-band magnitude $\lesssim 20$ are placed on the spectroscopic target list, and our follow-up observations are nearly complete out to that magnitude. Since the typical peak magnitude for a SN Ia with no extinction at redshift $z = 0.1$ is $r \simeq 19.3$, we might expect that the spectroscopic SN Ia sample should be essentially complete out to roughly this redshift as well; we shall see later that this is the case. This photometric preselection of SNe Ia has proven very effective: approximately 90% of the candidates initially targeted as SNe Ia after two or more epochs of imaging have resulted in a SN Ia spectroscopic confirmation. The SDSS-II Supernova Survey photometric classification and spectroscopic target selection are discussed in full detail in Sako et al. (2008).

[1]http://bruford.nhn.ou.edu/s̃uspect/index1.html

2.3. Artificial Supernovae

To measure the SN rate, it is clearly important to understand the efficiency of the survey for discovering SNe. As part of normal survey operations, we insert artificial SNe Ia (hereafter fakes) directly into the corrected survey images after the photometric reduction (`PHOTO`) but before difference imaging. The primary motivation for inserting fakes into the data stream is to provide real-time monitoring of the performance of the survey software pipeline and of the human scanning of objects. The fakes provide quantitative information about the efficiency of the survey software, human scanning, and the photometric classification of SNe Ia that is useful in the rate determination. Here we describe the basic algorithm for generating fakes and inserting them into the data stream; for more details, see Sako et al. (2008).

A fake is a pixel-level simulation of a point source with a light curve chosen to closely represent that of a real SN Ia. At each epoch for which the fake has a chance of being detected, the calculated CCD signal for the fake is directly added to the survey image. For the 2005 observing season, we generated a library of 874 fake light curves: each fake light curve is assigned a position, redshift, date of peak luminosity (in V-band), and an intrinsic luminosity that correlates with decline rate. This resulted in $\sim 7,800$ fake epochs during the season. The redshift distribution for the fakes was generated by assuming that the number of SNe Ia is roughly proportional to the volume element, $(dN/dz) \propto z^2$, in the range $0.0 < z < 0.4$.

To model the effect of contamination from host galaxy light on the detection efficiency, each fake is placed near a galaxy selected from the photometric redshift catalog (Oyaizu et al. 2007) for SDSS imaging on stripe 82. A host galaxy is drawn at random, from a distribution proportional to the r-band luminosity, from galaxies which have a photometric redshift within ~ 0.01 of the redshift assigned to the fake.

The SN Ia light curve model used to generate $ugriz$ magnitudes for a fake at each epoch is the same model that is used for early light curve fitting and photometric typing on the imaging data, but with the light curve parameters now chosen from an input probability distribution. To generate a point-source image from the ideal magnitudes, we use the estimate of the PSF from `PHOTO` at the position of the fake at the given epoch. We obtain the conversion from magnitudes to instrumental units (analog-to-digital units, or ADU) by running the `DoPHOT` photometry package on a set of cataloged stars in the survey image for which the magnitudes have been previously measured by the SDSS. After scaling the PSF model to match the computed ADU flux, we add Poisson fluctuations to each pixel. Finally, the row and column in the field that correspond to the position of the fake are taken from the astrometric solution provided by the imaging pipeline, and the fake is overlaid on the survey image.

When a fake is detected in the difference images, its identity as a fake is kept hidden while it is scanned by humans. After scanning, the fakes are revealed so that they are not mistakenly targeted for spectroscopic follow-up and so that the efficiency of scanners in tagging fakes as SN candidates can be monitored. However, like all candidates, fakes are processed through the automated light curve fitter/photometric typing algorithm so that we can test if they are accurately typed as SNe Ia after a few photometric epochs. The use of the fakes for measuring the survey detection efficiency is discussed in § 4.1.

2.4. Spectroscopy

The classification of SNe is defined by their spectroscopic features. In addition, spectroscopy provides a precise redshift determination and, in a number of cases, host galaxy spectroscopic-type information. Spectroscopic follow-up of the SDSS-II Supernova Survey candidates is being undertaken by a number of telescopes. During the 2005 observing season, spectroscopic observations were provided by the Hobby-Eberly 9.2m at McDonald Observatory, the Astrophysical Research Consortium 3.5m at Apache Point Observatory, the William-Herschel 4.2m, the Hiltner 2.4m at the MDM Observatory, the Subaru 8.2m and Keck 10m on Mauna Kea, and the SALT 11m at the South African Astronomical Observatory.

The classification of SN spectra is performed by comparing the spectral data to normal and peculiar supernova spectral templates from the work of Nugent et al. (2002) and to a public library of well-measured supernova spectra (Matheson et al. 2005; Blondin & Tonry 2007). The SN typing in this work is based on visual inspection of the spectra, but was guided by applying the cross-correlation technique of Tonry & Davis (1979) to the spectrum and the template library. The visual inspection relies heavily on the characteristic SN Ia features of Si and S absorption, which are usually prominent at optical wavelengths for this redshift range.

The redshift determination is based on galaxy features when they are present; otherwise SN features are used. In some cases, particularly at low redshift, a high-quality spectrum of the SN host galaxy is available from the SDSS-I spectroscopic survey. Comparison with those spectra indicate that our follow-up spectroscopic redshifts are determined to an accuracy of ~ 0.0005 when galaxy features are used and ~ 0.005 when SN features are used. Further details of the SDSS-II Supernova Survey first-season spectroscopic analysis are presented in Zheng et al. (2008).

2.5. Final Photometry

To obtain more precise SN photometry than the on-mountain difference imaging pipeline provides, we re-process the imaging data for all spectroscopically confirmed and other interesting SN candidates through a final photometry pipeline (Holtzman et al. 2008). In this "scene-modeling photometry" (SMP) pipeline, the supernova and the host galaxy (the *scene*) are modeled respectively as a time-varying point-source and a background that is constant in time, both convolved with a time-varying PSF. This model is constrained by jointly fitting all available images at the SN position, including images well before and after the SN explosion. Since there is no spatial resampling or convolution of the images that would correlate neighboring pixels, the error on the flux can be robustly determined. The SMP pipeline often provides photometric measurements at additional epochs compared to the survey operations pipeline. The final analysis of SN light curves discussed in this paper is based on SMP; in particular, the selection cuts described in §3 are made using the SMP pipeline.

3. Defining the SN Ia Sample for the Rate Measurement

The SN Ia sample for the rate measurement must include all SNe Ia in the redshift range of interest, not just those for which we have a confirming spectrum. Although we have high efficiency for discovering and spectroscopically confirming low-redshift SNe Ia (§3.1), we can take advantage of our rolling search data to carry out an extensive post-season hunt for SNe Ia that may have been missed by the search pipeline during the survey season (§3.2).

3.1. Spectroscopic SN Sample

In its first season (Fall 2005), the SDSS-II Supernova Survey discovered 130 events with secure spectroscopic identifications as SNe Ia[2] and 16 events that are considered probable SNe Ia based on their spectra. For SN Ia events satisfying the selection criteria below, the spectroscopic follow-up is essentially complete for redshifts $z \leq 0.12$, so we have chosen to focus on this redshift range for a first measurement of the SN rate. For $z \leq 0.12$, the sample contains 27 spectroscopically confirmed SNe Ia and 2 spectroscopically probable SNe Ia before making selection cuts.

For the measurement of the SN Ia rate, we impose a number of selection criteria on

[2]The classification of 2005gj as a SN Ia may be controversial (Prieto et al. 2007); as noted in §1, we exclude it from this analysis.

the SN photometric data, with the aim of producing a sample that has a well-characterized selection function. These criteria are applied to the spectroscopically confirmed and probable SNe Ia with $z \leq 0.12$. For consistency, we will also apply these selection cuts to the photometric (i.e., spectroscopically unconfirmed) SN sample discussed in §3.2. The selection cuts for the rate measurement are as follows:

1. $-51^\circ < \alpha_{J2000} < 57^\circ$.

   Although the SDSS-II Supernova Survey covers the RA range $-60^\circ < \alpha_{J2000} < 60^\circ$, early in the Fall 2005 observing season we did not have complete templates available for the regions $\alpha_{J2000} < -51^\circ$ and $\alpha_{J2000} > 57^\circ$, so these RA regions were not initially used for the SN search, as shown in Fig. 1. In principle, we could account for this by modeling the time-varying effective search area, but for simplicity we choose to excise these RA regions from the rate measurement. Furthermore, the calibration star catalog used by our final photometry pipeline (Ivezić et al. 2007) does not extend below $\alpha_{J2000} \sim -51^\circ$, and we cannot presently simulate light curves for SNe in this region. This cut removes one confirmed SN Ia, 2005iu, from the rate sample.

2. There are photometric observations on at least five separate epochs between -20 days and $+60$ days relative to peak light in the SN rest-frame.

   Peak light refers to the date of maximum luminosity in the SN rest-frame B-band according to the best-fit MLCS2k2 light curve model. This cut requires that the light curve is reasonably well-sampled and it is primarily useful for photometrically distinguishing SNe Ia from other SN types with high confidence when there is no SN spectrum available (see §3.2). Here and below, a photometric observation simply means that the survey took imaging data at that epoch on that region of sky and that SMP reported a SN flux measurement (not necessarily significant or even positive) with no error flags (see Holtzman et al. (2008)) in at least one of the three *gri* passbands. It does *not* imply a detection above some signal-to-noise threshold. One SN discovered late in the observing season, 2005lk, fails this cut.

3. At least one epoch with signal-to-noise ratio > 5 in each of g, r, and i (not necessarily the same epoch in each passband).

   This cut ensures that there are well-measured points on the light curve, and is mainly useful for rejecting low signal-to-noise events from the photometric sample. All spectroscopically confirmed SNe Ia in the low-redshift sample satisfy this cut.

4. At least one photometric observation at least two days *before* peak light in the SN rest frame.

5. At least one photometric observation at least ten days *after* peak light in the SN rest frame.

   These two cuts require sampling of the light curve before and after peak light, ensuring that we have a precise determination of the time of peak light. These cuts also help remove non-SN Ia contaminants from the photometric sample (see §3.2). Finally, they guarantee that the epoch of peak light occurs during our observing season, i.e., between Sept. 1 and Nov. 30, which is one of the criteria used in defining the rate measurement in §5. Since these cuts are *more* restrictive than the requirement of peak light during the observing season, they are the main contributors to the inefficiency estimated in §4.2. These are the most restrictive cuts on the spectroscopic SN Ia sample, together removing nine events: four SNe Ia discovered early in the observing season do not have a pre-maximum observation, and five SNe Ia found late in the season do not have a photometric observation more than ten days past peak light.

6. MLCS2k2 light curve fit probability > 0.01.

   The MLCS2k2 light curve fitter (Riess et al. 1996; Jha et al. 2007) takes as input the measured SN magnitudes in each passband at each epoch, and the measured SN redshift; it then finds the likelihood as a function of the four parameters μ (the distance modulus), A_V (the extinction parameter), the time of peak light in rest-frame B-band, and the light curve shape/luminosity parameter Δ. The MLCS2k2 fit probability is defined by evaluating the usual χ^2 statistic for the data and the best fitting MLCS model and assuming that this statistic obeys a χ^2_{n-4} probability distribution, where n is the number of photometric data points. The model parameters of the best fitting MLCS2k2 model are defined as the mean of the probability distribution for each corresponding parameter. This cut on the fit probability provides an automated method of removing photometrically peculiar SNe Ia from the sample. We find that essentially all of the spectroscopically normal SNe Ia in our confirmed sample have a fit probability > 0.1. However, the spectroscopically confirmed SN Ia sample is likely to be biased toward "high-quality" light curves, so we place the selection cut at a less restrictive value. Three spectroscopically identified SNe Ia are rejected by this cut, including the peculiar SNe 2005hk (χ^2/d.f. = 90/21) and 2005gj (χ^2/d.f. = 198/45). The third rejected SN, with internal SDSS candidate designation 6968 (χ^2/d.f. = 78/27), was classified as a spectroscopically probable SN Ia (see §2.4) and shows some evidence of being spectroscopically similar to 2005hk. For the sample of photometric SN candidates (§3.2), this cut helps remove non-SN astrophysical variables, such as AGN and M stars.

7. MLCS2k2 light curve fit parameter $\Delta > -0.4$.

The MLCS parameter Δ is a measure of the light curve shape and intrinsic luminosity. Smaller values of the Δ parameter correspond to more slowly-declining, intrinsically brighter SNe Ia. This cut requires that Δ be consistent with the values observed for the low-redshift SNe Ia that were used to train the MLCS2k2 light curve fitter. For the photometric SN candidates, this cut helps reject Type II supernovae, which often have a long plateau after the epoch of peak luminosity and result in large negative fitted values of Δ.

The above selection requirements result in the 16 spectroscopically identified SNe Ia that are listed in Table 1. This sample includes 2005je, which was classified as spectroscopically probable. The spectroscopically confirmed SNe Ia that are removed from the rate-measurement sample are listed in Table 2; the last column indicates which of the above selection criteria was used to remove each SN.

Table 1. SNe Ia included in the rate sample.

SDSS Id	IAUC Designation	α (J2000.0)	δ (J2000.0)	Redshift	Redshift Source
1241	2005ff	22 30 41.41	−00 46 35.7	0.088	SN
1371	2005fh	23 17 29.71	+00 25 45.8	0.120	galaxy
2561	2005fv	03 05 22.42	+00 51 30.1	0.119	galaxy
3256	2005hn	21 57 04.23	−00 13 24.4	0.107	galaxy
3592	2005gb	01 16 12.58	+00 47 31.0	0.086	galaxy
3901	2005ho	00 59 24.10	+00 00 09.3	0.063	galaxy
5395	2005hr	03 18 33.81	+00 07 24.3	0.117	SN
5549	2005hx	00 13 00.13	+00 14 53.7	0.120	SN
5944	2005hc	01 56 47.94	−00 12 49.1	0.046	galaxy
6057	2005if	03 30 12.87	−00 58 28.5	0.067	galaxy
6295	2005js	01 34 41.51	−00 36 19.4	0.084	SN
6558	2005hj[a]	01 26 48.40	−01 14 17.3	0.057	—
6962	2005je	02 35 26.61	+01 04 29.6	0.094	galaxy
7147	2005jh	23 20 04.42	−00 03 19.8	0.109	galaxy
7876	2005ir	01 16 43.80	+00 47 40.7	0.076	galaxy
8719	2005kp	00 30 53.15	−00 43 07.9	0.117	galaxy
9266[b]	—	03 20 43.16	−01 00 07.2	0.036	galaxy

[a]SN type confirmed by Quimby et al. (2005)

[b]Photometrically identified SN Ia. See §(3.2)

Note. — SDSS Id denotes internal candidate designation.

Table 2. Spectroscopically confirmed SNe Ia with $z \leq 0.12$ cut from the rate sample.

SDSS Id	IAUC Designation	α (J2000.0)	δ (J2000.0)	Redshift	Cut Index
722	2005ed	00 02 49.37	+00 45 04.6	0.086	4
739	2005ef	00 58 22.87	+00 40 44.6	0.107	4
774	2005ex	01 41 51.24	−00 52 35.0	0.093	4
2102	2005fn	20 48 53.04	+00 11 28.1	0.095	4
4524	2005gj	03 01 11.95	−00 33 13.9	0.062	6
6773	2005iu	20 20 15.61	+00 13 02.5	0.090	1
6968	—	01 18 13.37	−00 54 23.6	0.098	6
8151	2005hk	00 27 50.88	−01 11 53.3	0.013	6
10028	2005kt	01 10 58.04	+00 16 34.1	0.066	5
10096	2005lj	01 57 43.03	−00 10 46.0	0.078	5
10434	2005lk	21 59 49.43	−01 11 37.3	0.103	5,2
10805	2005ku	22 59 42.61	−00 00 49.3	0.045	5
11067	2005ml	02 14 04.42	−00 14 21.1	0.119	5

Note. — SDSS Id denotes internal candidate designation. See section 3.1 for explanation of cut index.

3.2. Photometric SN Sample

In addition to the spectroscopically identified SNe Ia discussed above, the survey has measured light-curves for a few thousand variable objects, including possible SNe, for which we did not obtain a classifiable spectrum while the source was bright enough to identify. We refer to these spectroscopically unobserved or unclassified objects as *photometric SN candidates*. There are a number of reasons for such spectroscopic incompleteness, including limited spectroscopic resources, targeting errors (e.g., misplacement of a spectroscopic slit), poor weather either preventing spectroscopic observations or rendering them indeterminate, and possible inefficiencies in the spectroscopic target selection algorithm. In order to make a reliable SN Ia rate measurement, we must investigate the photometric SN candidates to determine the level of incompleteness, if any, of the spectroscopic SN Ia sample. This is a challenge, because a sample of purely photometric SN Ia candidates may be heavily contaminated by objects that are not SNe Ia, especially if there are significant numbers of objects with multi-band light curves that are not too dissimilar from those of SNe Ia. The combination of selection cuts listed in §3.1 is designed to meet this challenge, by rejecting the majority of non-SN Ia contaminants. In addition to the spectroscopically confirmed and spectroscopically probable SNe Ia discussed in §3.1, the SDSS-II Supernova Survey discovered 16 low-redshift SNe that were spectroscopically confirmed as non-Ia SNe in it's first year. As a check that our selection cuts are effective at rejecting non-Ia SNe, we apply the same cuts to this sample of 16 low-redshift ($z < 0.2$) spectroscopically confirmed non-Ia SNe. All but one of these non-Ia SNe are rejected by these selection cuts. The selection criteria above could be made more restrictive in order to reduce potential non-Ia contamination of the photometric SN sample. For example, by requiring a photometric observation at least 16 (as opposed to 10) days after peak light in the SN rest frame, the spectroscopic non-Ia SN above would be eliminated from the sample. However, we find that such a change would have no impact on the selection of photometric SN candidates for inclusion in the rate sample.

To determine whether any of the photometric SN candidates are genuine SNe Ia in the redshift range of this rate measurement, we must estimate both the SN type and redshift for each candidate. There are two categories of photometric SN candidates, (a) those for which we have a precise spectroscopic measurement of the redshift and (b) those for which we do not. The redshifts for category (a) candidates come from two sources. The first source is the SDSS-I spectroscopic galaxy survey, which measured redshifts for $\sim 28,000$ galaxies in our survey region at redshifts $z \leq 0.12$. The second source is from subsequent spectroscopic observations of ~ 80 host galaxies of the highest-quality photometric SN candidates; these spectra were obtained in the summer and fall of 2006 and 2007. Using the sample selection process described below in §3.2.2, we found in our imaging data only one photometric SN Ia candidate that passes the selection criteria in §3.1 and that has a spectroscopic redshift

$z \leq 0.12$ (category (a)). The host galaxy of this SN Ia candidate, which has internal SDSS SN designation 9266, has a spectroscopic redshift of $z = 0.0361$ measured by the SDSS galaxy redshift survey. This object was not targeted for spectroscopic follow-up during the SDSS-II Supernova Survey because it has very high extinction, $A_V \simeq 4$ according to the MLCS2k2 fit. This extinction value lies outside the range of the A_V-search grid for the photometric typing algorithm used during the search (§2.2).

3.2.1. Redshift estimation for photometric SN candidates

For each photometric SN candidate *without* a spectroscopically determined redshift (category (b) above), we must estimate both the redshift and the SN type from the photometric data. We do this using a modification of the standard MLCS2k2 light curve fit, in which the redshift is included as a parameter in the likelihood function. In this instance, the distance modulus μ is *not* treated as a fit parameter; instead, we adopt the concordance LCDM cosmology, with $\Omega_m = 0.3$, $\Omega_\Lambda = 0.7$, and dark energy equation of state parameter $w = -1$, and fix $\mu(z)$ to its functional form for that cosmology. The photometric redshift estimate z_{phot} is then obtained by marginalizing over the other fit parameters, i.e., the epoch of peak luminosity, the extinction A_V, and the shape parameter Δ.

Although these SN photometric redshift estimates depend on the assumed cosmology, we do not expect them to be extremely sensitive to the values of the cosmological parameters, especially at the modest redshifts under consideration here. To test the accuracy of these redshift estimates, we applied the MLCS2k2 redshift fit to SNe Ia light curves that have spectroscopically measured redshifts. For this test, we use two sets of objects: (i) all spectroscopically confirmed SNe Ia with redshift $z \leq 0.25$, and (ii) all photometric SN Ia candidates that satisfy the selection criteria in §3.1 and that have spectroscopic (host galaxy) redshift $z \leq 0.25$. We include objects in category (ii) because the spectroscopically confirmed SNe Ia could represent a biased sample of the SN Ia population if there are spectroscopic selection biases. We include objects with redshift $z > 0.12$ to yield a more statistically significant test and to check for photometric redshift biases that could cause these objects to be erroneously included in the $z \leq 0.12$ sample. There are 61 and 28 events in categories (i) and (ii), respectively.

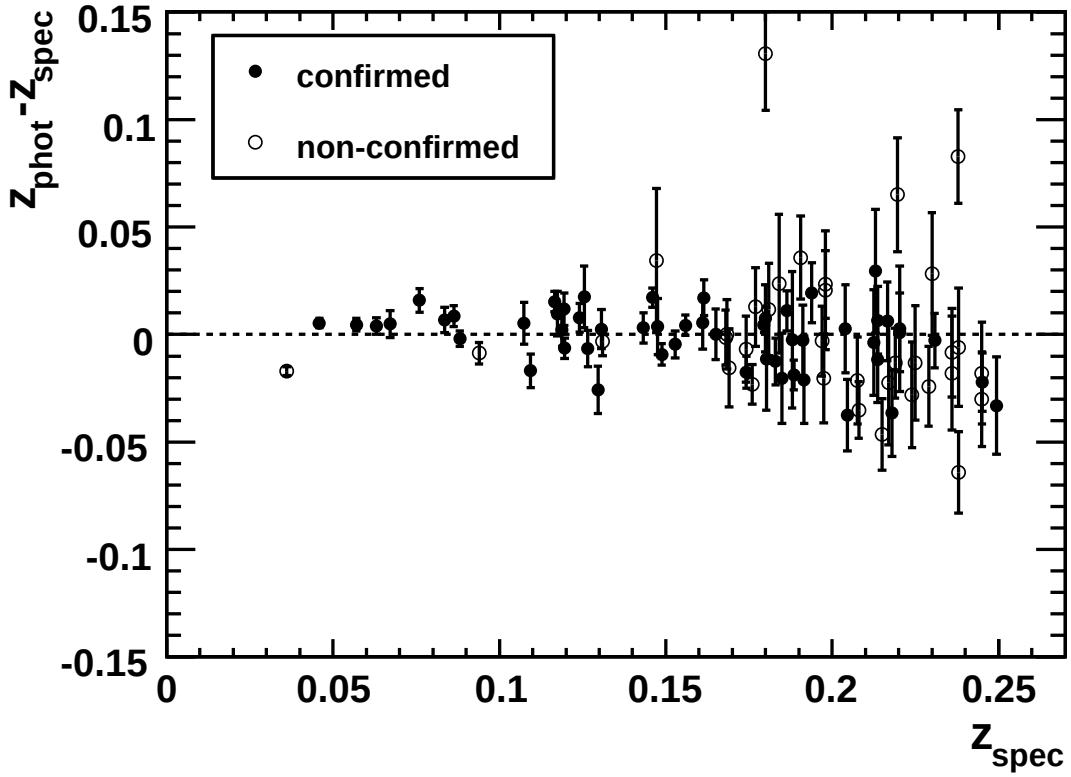

Fig. 2.— Residuals of the photometric redshift estimates, $z_{phot} - z_{spec}$ vs. z_{spec}, for the sample of spectroscopically confirmed SNe Ia (black points) and for the photometric SN Ia candidates that satisfy the rate selection cuts and for which host galaxy redshifts are available (open points). The marginalized redshift errors reported by the MLCS2k2 light-curve fits are shown.

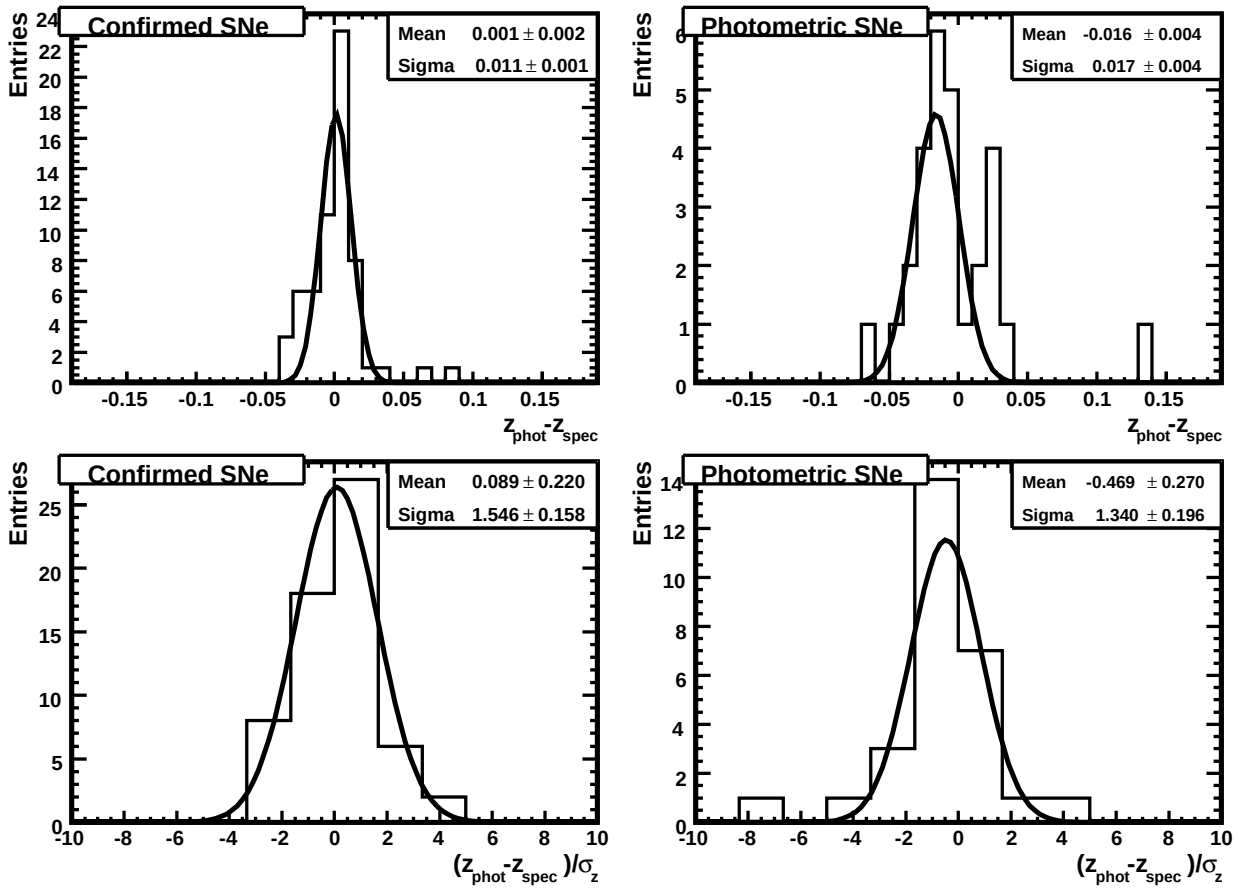

Fig. 3.— The distribution of photometric redshift residuals for the spectroscopically confirmed SNe Ia (left panels) and the photometric SN Ia candidates (right panels) shown in Fig. 2. Upper panels show distributions of the difference between the photometric redshift, z_{phot}, and the spectroscopic redshift, z_{spec}; lower panels show distributions of $(z_{phot} - z_{spec})/\sigma_z$, where σ_z is the photometric redshift uncertainty reported by the MLCS2k2 fit. Inset panels show the inferred mean and dispersion of the Gaussian fits to each distribution.

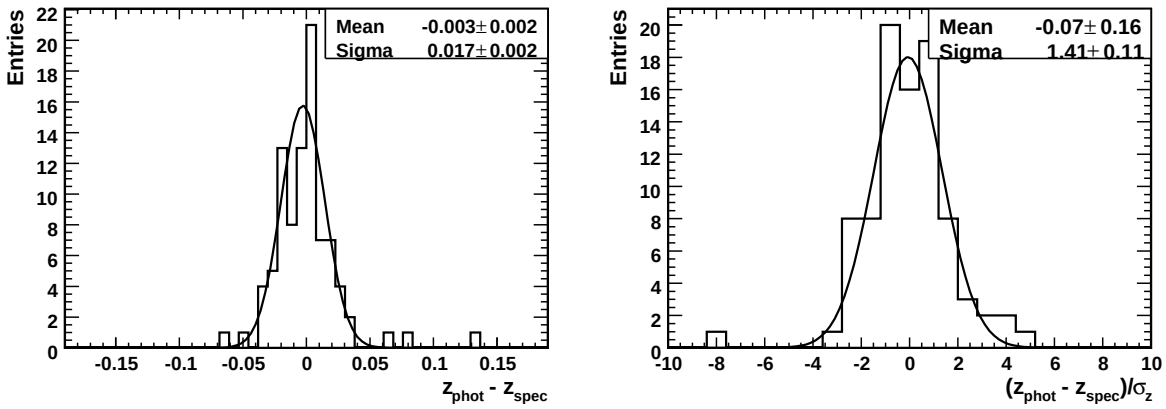

Fig. 4.— *Left panel:* The distribution of photometric redshift residuals, $z_{phot} - z_{spec}$, for the combined spectroscopic+photometric SN Ia samples. z_{phot} is the photometric redshift and z_{spec} the spectroscopic redshift; *Right panel:* distribution of residuals normalized by the reported photometric redshift uncertainty, σ_z.

The residuals of the SN photometric redshift estimates for this test sample of 89 objects are shown in Figure 2. The distributions of the residuals are shown in Figure 3 separately for categories (i) and (ii), which indicates that the distributions for the two samples are consistent. The fit residuals for the combined sample are shown in Figure 4. For the combined sample, the mean residual of the photometric redshift estimate is consistent with zero. The scatter in the photometric redshift estimate for the combined test sample is $\sigma_z = 0.018$, and Fig. 2 shows that the scatter increases with redshift. The distribution of the residuals normalized by the MLCS-reported redshift error is shown in the right panel of Figure 4. If the reported redshift errors were accurate and Gaussian, this distribution would be a Gaussian with unit variance, $\sigma = 1$. The distribution appears to be approximately Gaussian, but with measured variance $\sigma = 1.4$; we therefore choose to multiply the MLCS-estimated photometric redshift error for each candidate by 1.4.

In addition to the SN photometric redshift estimates, we also have host galaxy photometric redshift estimates for the majority of photometric SN candidates (Oyaizu et al. 2007). Although the galaxy z_{phot} estimates have larger scatter than those from the SN light curves, in principle we could require consistency between these two redshift estimates as an additional selection cut on the photometric SN sample. Since core-collapse SNe are typically fainter than SNe Ia, they would typically be assigned incorrectly high photometric redshifts by the light curve fitter. Using the existing selection cuts, however, we find no contamination of the rate-measurement sample from the photometric SN candidates without spectroscopic redshifts (see §3.2.2). Therefore a requirement of consistency between the supernova- and galaxy-derived photometric redshift estimates is not necessary in the present analysis.

3.2.2. Selection of photometric SN candidates

In the Fall 2005 observing season, the software and human data processing pipeline described in §2.2 yielded 11,385 SN candidates, including the 146 spectroscopically confirmed and probable SNe Ia and 20 that were confirmed as other SN types. The majority of the remaining candidates ($\sim$ 60%) are single epoch events that are most likely to be slow-moving asteroids, leaving $\sim$ 4500 multi-epoch SN candidates. To search for photometric SNe Ia among this large set of candidates, we studied two subsamples selected according to different criteria.

The first photometric subsample is designed to exhaust the list of candidates that are most likely to be SNe Ia. This subsample was selected by choosing all SN candidates that

the survey photometric typing code (described in §2.2) classified as SNe Ia[3] and that were detected in at least 3 epochs by the on-mountain software pipeline. The images for the resulting subsample of $\sim$ 420 candidates were processed through the final SMP pipeline, and the resulting light curves were fit with the MLCS2k2 program, using the redshift as a fit parameter in cases where there was no measured host galaxy spectroscopic redshift (the majority of cases). One highly extincted SN Ia (SDSS-SN 9266, discussed in §3.2), with a host galaxy redshift measured by the SDSS galaxy survey, was recovered from this subset of photometric SN candidates. No other candidates in this subsample pass the rate selection cuts and have a spectroscopic or SN photometric redshift $z \leq 0.12$.

The second photometric subsample is designed to study the candidates that are less likely to be SNe Ia. This subsample was selected by choosing all SN candidates with detections at more than two epochs during the search and with an estimated time of maximum light, based on the survey photometric typing code, in the twenty-day interval between modified Julian day (MJD) of 53660 and 53680 (October 17 and November 6). Since the selection criteria for this second subsample are looser than for the first (there is no requirement that a SN Ia light-curve template provides the best-fit), the number of candidates it selects would be an order of magnitude larger. Using a restricted time interval provides a manageable number of events to study that are representative of the population of these lower-quality light curves. These selection criteria result in 462 candidates, which represent $\sim 1/6$ of the multi-epoch SN candidates that have not already been included in the samples discussed above. We find no events in the second subsample that pass the rate measurement selection cuts and that have a spectroscopic or SN photometric redshift $z \leq 0.12$.

Although no other photometric SN candidates pass our selection criteria, we must allow for uncertainties in the SN photometric redshift estimates from MLCS2k2. In the two photometric subsamples, two candidates that pass the rate-selection cuts have estimated SN photometric redshifts within $\sim 1.5\sigma$ of our cutoff of $z = 0.12$, using the inflated redshift errors discussed in §3.2.1. One of these candidates is from the first photometric subsample and has a fitted redshift 0.17 ± 0.03 (SDSS-SN internal ID 3077); the second is from the second photometric subsample and has a fitted redshift of 0.18 ± 0.04 (SDSS-SN ID 6861). Efforts are underway to obtain spectroscopic redshifts for the host galaxies of these events. Interpreting the (inflated) photometric redshift errors as Gaussian (§3.2.1), the probability that at least one of these two candidates has a redshift $z \leq 0.12$ is significantly less than unity. To be conservative, we assign a systematic uncertainty of +1 SN Ia based on this study.

[3]More precisely, according to the photometric typing code, one of the "type A" or "type B" criteria were satisfied; see Sako et al. (2008)

3.3. Summary of Rate Sample Selection

In summary, rate-sample selection requirements have been applied to SN candidates with $z \leq 0.12$ from the 2005 observing season. The resulting sample comprises 16 spectroscopically identified and 1 photometrically identified SNe Ia. These events are enumerated in Table 1, and their *gri* light curves are shown in Figure 5 along with the best-fit MLCS2k2 model light-curve. Figure 6 shows the redshift distribution for SNe Ia for $z \leq 0.21$; the lowest-redshift photometric candidates with no spectroscopic redshift are in the bin $0.15 < z < 0.18$ and are safely above the redshift cut.

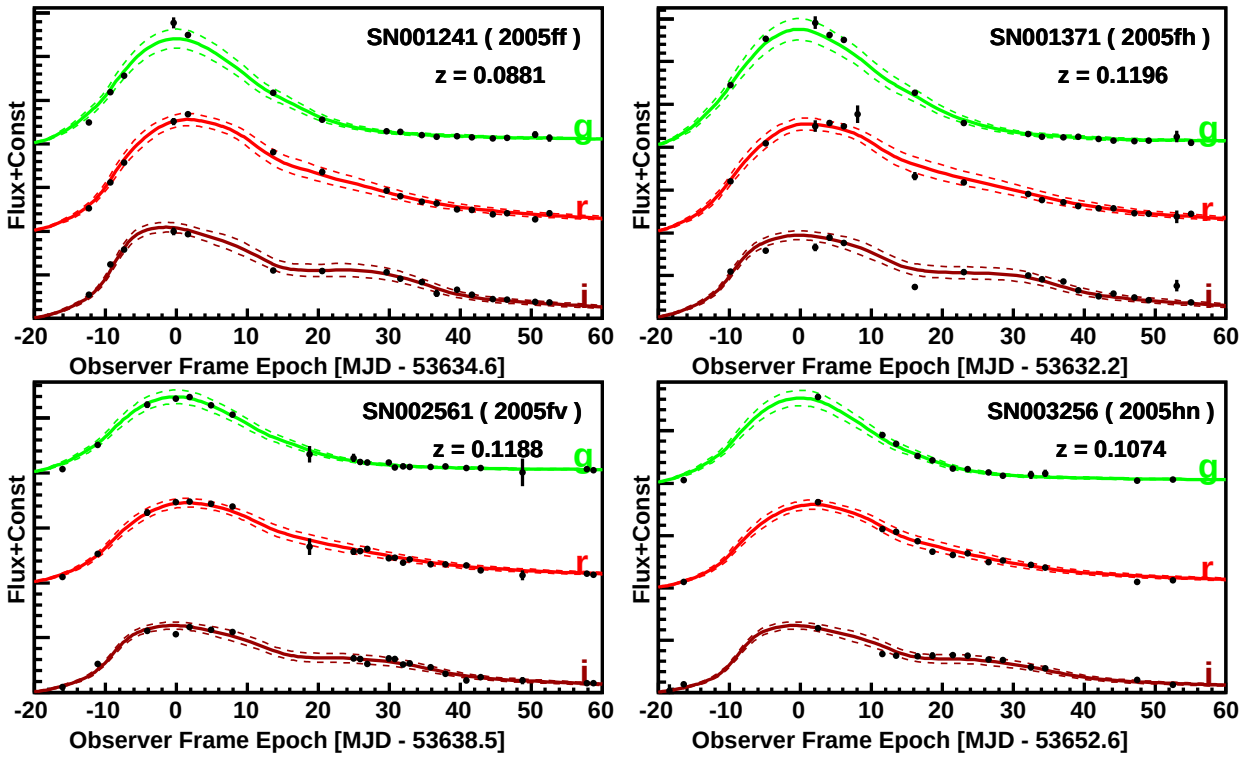

Fig. 5.— *gri* light curves for SNe Ia used in this rate measurement. Black points show the SDSS SN photometry from SMP. The errors on the photometry are shown. Solid curves denote the best-fit SN Ia model light curves in g (green), r (red), and i (dark red) from the MLCS2k2 light-curve fitter, and corresponding dotted curves show the 1-sigma model error range. The curves and data for the different passbands have been vertically offset for clarity. The flux offsets are the same for each SN.

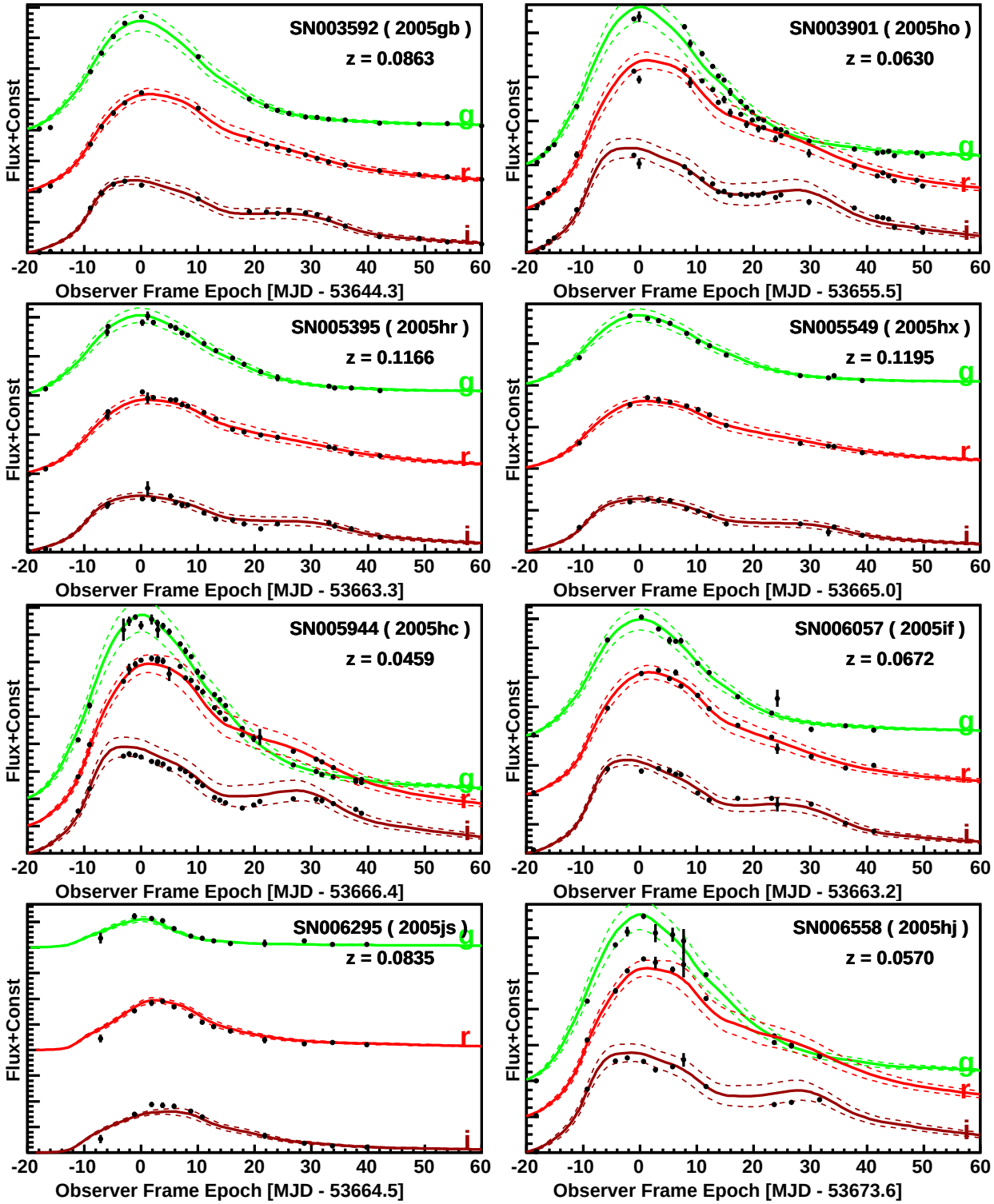

Fig. 5. — Continued.

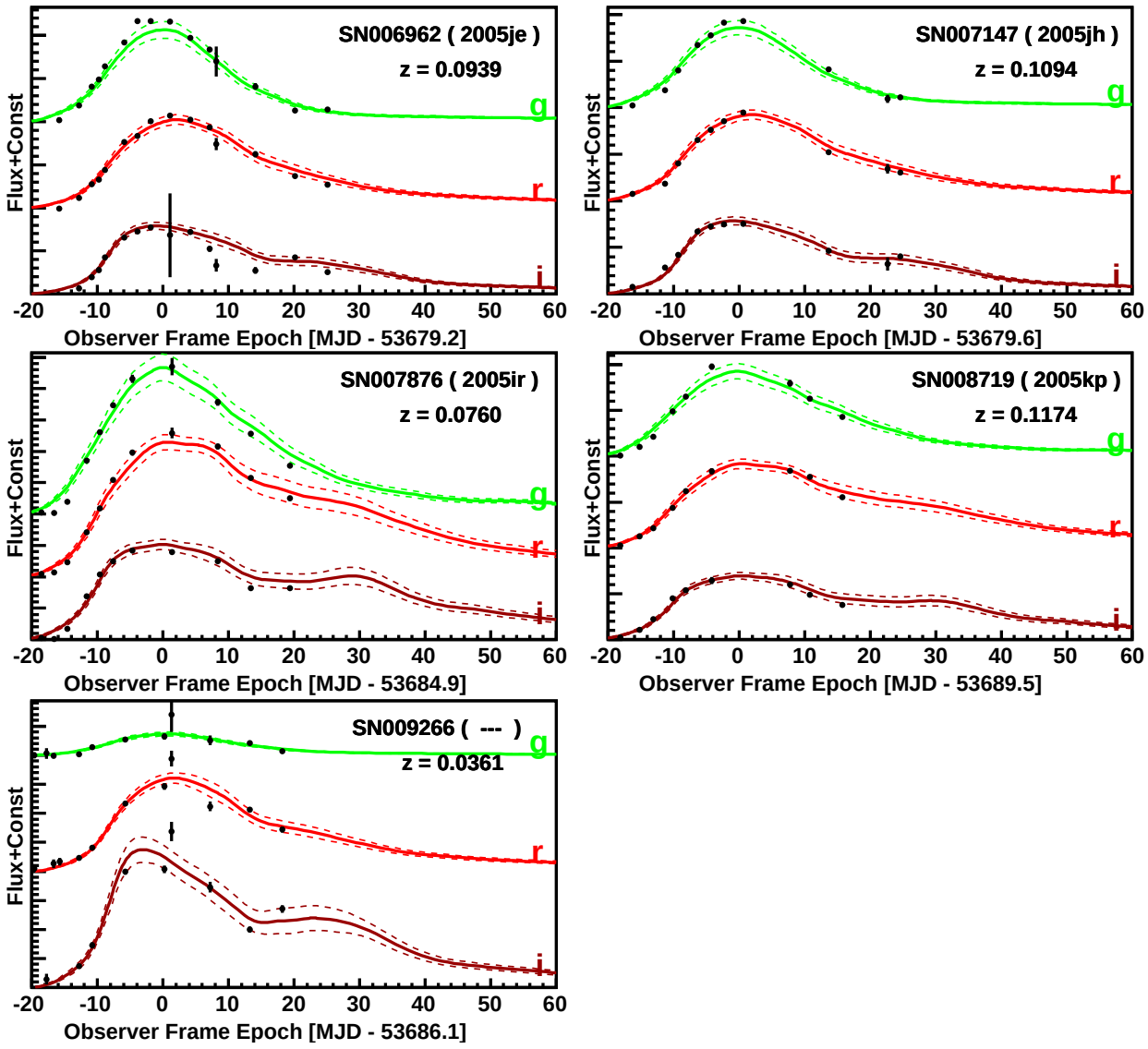

Fig. 5. — Continued.

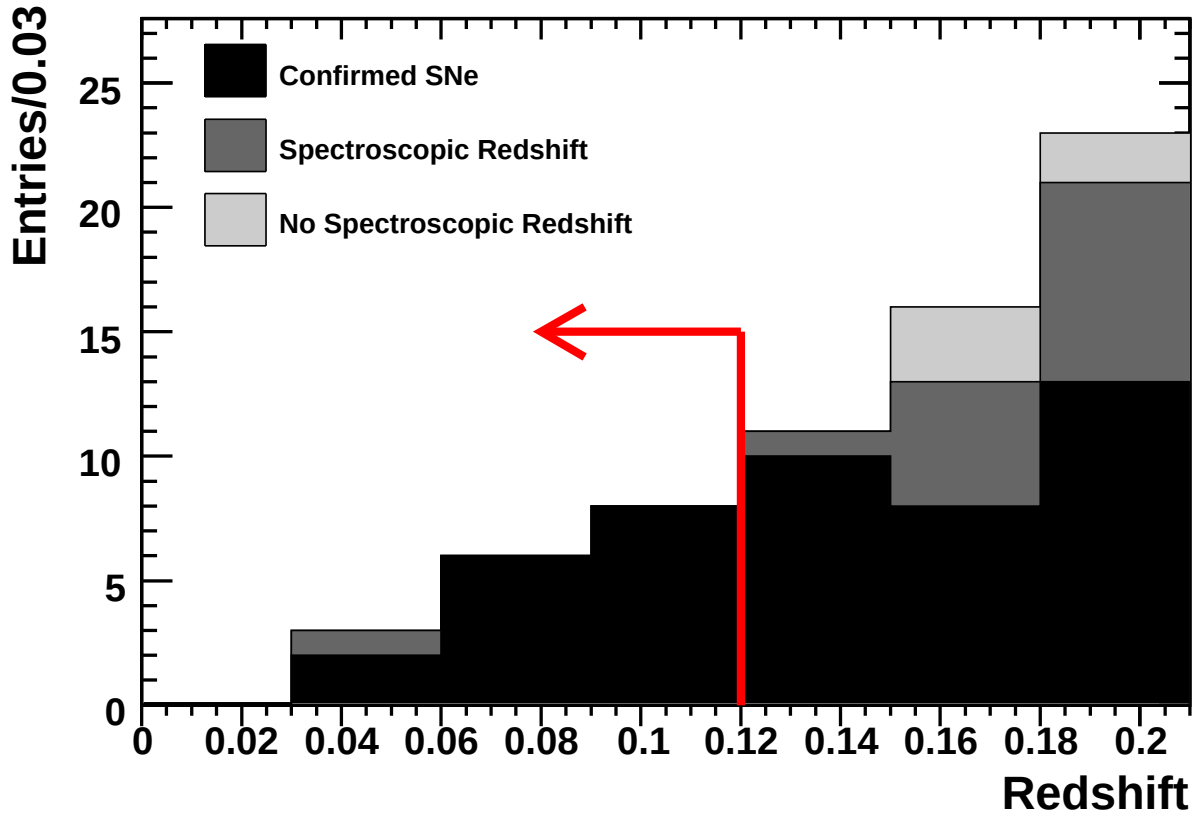

Fig. 6.— Redshift distribution for events passing the rate-measurement selection requirements in §3.1. Contributions include: spectroscopically confirmed SNe Ia (black), photometric SNe Ia with host galaxy redshifts (gray), and photometric SN Ia candidates with no spectroscopic redshift (light-gray). The arrow shows the redshift cut for this analysis.

4. Survey Efficiency

To convert the number of discovered SNe Ia into a measurement of the SN rate, we must have an estimate of the efficiency for discovering SNe Ia at $z \leq 0.12$ that satisfy the sample selection criteria. We have two tools at our disposal for this estimate: the artificial SN images (fakes) that are inserted into the data stream in real time and Monte Carlo simulations of the 2005 observing season.

4.1. Use of Artificial SN Images

As noted in §2.3, the fake SNe images are used to measure the efficiency of the on-mountain software pipeline for point-object detection on a variety of galaxy backgrounds and observing conditions. The fake SNe are also used to measure the efficiency of human scanners for identifying objects as SNe. While the fakes were designed to model realistic SN Ia light curves, the z^2 dependence on the redshift distribution results in only 18 fake light curves with redshift $z < 0.12$. Although all 18 low-redshift fakes were recovered by the SN search pipeline, using such a small sample to measure the pipeline efficiency would result in large statistical and systematic uncertainties. Furthermore, the fake light curves were generated with distributions of A_V and Δm_{15} that were not realistic, which complicates the interpretation of discovery efficiency as a function of redshift.

To obtain a more reliable determination of the survey efficiency, we use fake SN Ia at all redshifts in the following way. We first use the fakes to measure the object-detection efficiency as a function of the signal-to-noise ratio (SNR) in the g, r, and i passbands. The detection efficiency, defined as the ratio of the number of fake epochs detected as objects by the on-mountain software pipeline to the number of fakes inserted into data images at a given signal-to-noise, is shown in Fig. 7. While the object detection efficiency as a function of magnitude or redshift is sensitive to observing conditions (seeing, clouds, moon), the efficiency as a function of SNR is robust against such variations in conditions. As a check that the SNR is an adequate parameterization of the point-source detection efficiency, we have split the sample of fakes into a low-redshift and a high-redshift subsample and determined the efficiency as a function of SNR for each set independently. We find that the results are consistent. With the efficiency as a function of signal-to-noise ratio known, one can estimate the SN discovery efficiency as a function of redshift for *any* choices of SN Ia light-curve models, observing conditions, and population distributions. These efficiency functions measured with fakes are used in the Monte Carlo simulation (§4.2) to verify that the software pipelines were fully efficient at low redshift.

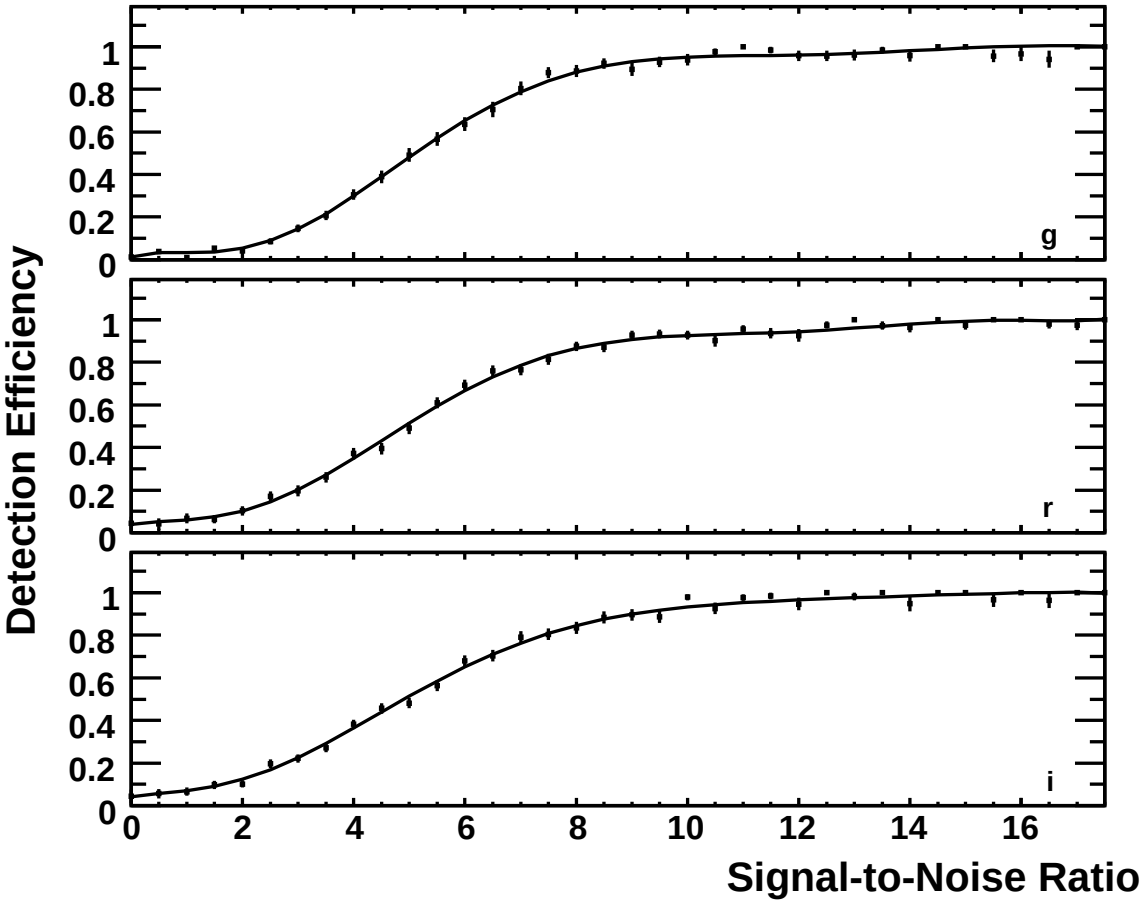

Fig. 7.— The mean object detection efficiency as a function of signal-to-noise ratio for SDSS g-band (top), r-band (middle), and i-band (bottom). The efficiency is derived by counting the fraction of fake images detected by the survey pipeline. The binomial errors on the efficiency measurements are shown. The solid lines show the result of a polynomial fit to the efficiency measurements. These efficiency functions are used to simulate the difference imaging software in the Monte Carlo simulations of the SN light curves.

The fakes also provide information on the efficiency of the human scanners to correctly label as possible SN candidates those fakes that were detected as objects by the software pipeline. For the 2005 season, 91% of all epochs of fakes visually scanned by humans were flagged as SN candidates, and 95% of all detected fake SNe were flagged by humans as SN candidates at least once. The 5% of fakes that were never identified by humans as SN candidates were detected on only a single epoch by the software pipeline, either because they were at high redshift or because they reached peak light well before or well after the observing season. Essentially all fakes detected on two or more epochs by the software pipeline were flagged by humans as SN candidates at least once. Given the selection cuts in §3.1, the human scanning efficiency is 100% for SNe Ia contributing to this low-redshift rate measurement.

Summary information on the efficiency of the software pipeline and the human scanners to detect fakes is presented in Figure 8, which shows the detection efficiencies, i.e., the fraction detected by the pipeline and the fraction identified as SN candidates by humans, vs. peak g-magnitude. The arrows indicate the peak g-band magnitudes for an unextincted normal and for an unextincted sub-luminous 1991bg-like SN Ia at $z = 0.12$, according to the MLCS2k2 model. This figure indicates that, for the assumed SN Ia model used to generate the distribution of fakes, the combined software+human detection efficiency is essentially 100% for SNe Ia in the redshift range $z \leq 0.12$.

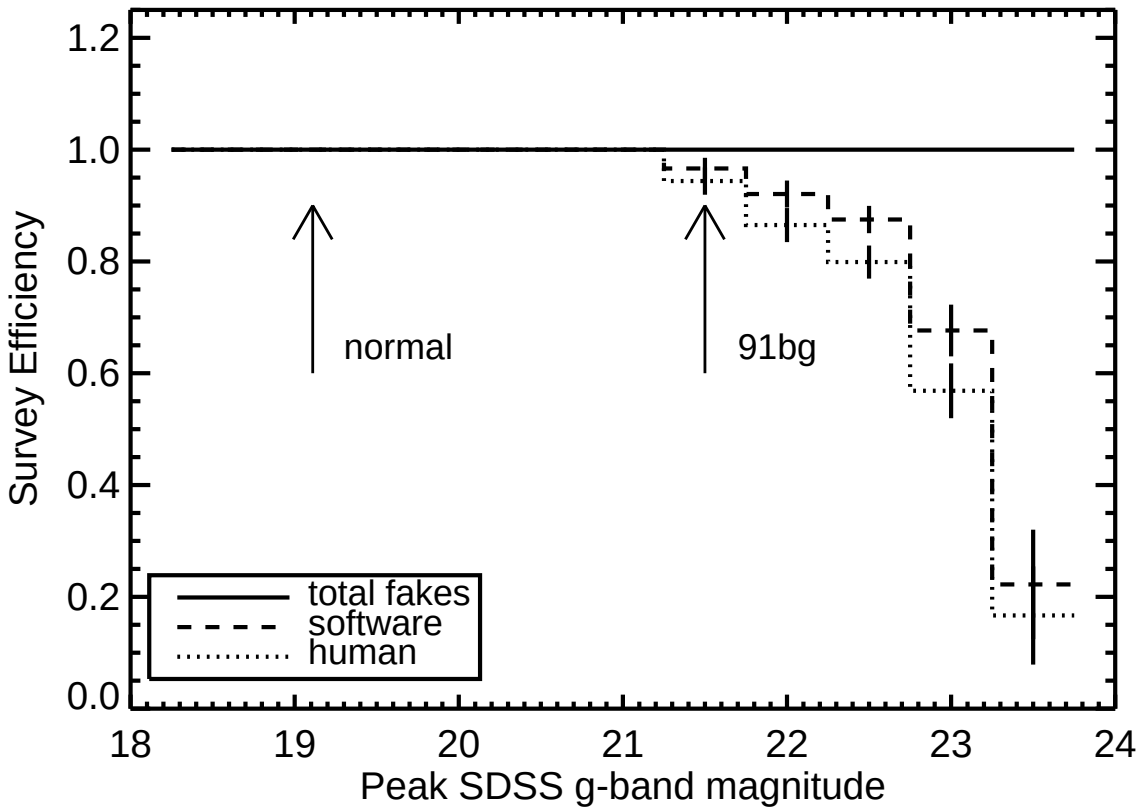

Fig. 8.— The efficiency for identifying fakes as SN candidates, as a function of peak g-band magnitude. The dashed curve is the efficiency for detection by the software pipeline, and the dotted curve is the efficiency for evaluation of the fakes as SN candidates by the human scanners. The arrows indicate the peak magnitudes for a normal and for a 91bg-like SN Ia at a redshift of 0.12 according to the MLCS2k2 model. The binomial errors on the efficiency are shown.

4.2. Monte Carlo Simulations

To determine the SN Ia selection efficiency with high precision and to study systematic uncertainties for the rate measurement, we have developed a detailed Monte Carlo light curve simulator (MC). The MC simulates individual light curve data points based on real observing statistics, but without the added complexity of adding fake SNe to images. The MC light curves can be generated and analyzed much more rapidly than the fakes, so the MC can be used to rapidly simulate very large numbers of SN Ia light curves to estimate the SN discovery efficiency and the uncertainty in the efficiency due to assumptions about the SN Ia model distributions. The MC code uses the MLCS2k2 model to generate simulated SN Ia light curves instead of the stretch/Δm_{15} model that was used to generate the fakes.

For each simulated SN Ia, the following parameters are randomly drawn from parent distributions:

1. **redshift, z:**
   Drawn from a distribution proportional to the comoving volume element, which assumes a constant SN Ia rate per unit comoving volume.

2. **host galaxy extinction, A_V:**
   Drawn from a distribution $P(A_V) \propto e^{-A_V/\tau}$, with $\tau = 0.4$. The Cardelli et al. (1989) reddening law, with $R_V = 3.1$, is used to extrapolate the extinction to other wavelengths. The choice of $\tau = 0.4$ was guided by the studies of Jha et al. (2007) and is consistent with the inferred extinction distribution for spectroscopically confirmed SNe Ia in the SDSS SN sample. As we discuss later in this section, the exact choice of τ makes no practical difference to this rate measurement.

3. **MLCS2k2 light curve shape/luminosity parameter, Δ:**
   Drawn from a bimodal Gaussian with a standard deviation of 0.26 for $\Delta < 0$ and 0.12 for $\Delta > 0$, and truncated to lie within the valid range of the MLCS2k2 model, $-0.35 < \Delta < 1.8$. The bimodal Gaussian is based on study of the confirmed SNe Ia in the SDSS-II Supernova Survey first year data.

4. **time of peak light in rest-frame B-band:**
   Drawn randomly from the interval 53616 < MJD < 53705 (Sept. 1 - Dec. 1, 2005).

5. **sky position:**
   Drawn randomly from the range of the survey.

6. **location within host galaxy:**
   Drawn from a distribution proportional to the host galaxy surface brightness (see

below). This variable is used only to determine galaxy background light, not extinction.

We note that simulated photometry is generated only at epochs for which we obtained photometric imaging at the corresponding sky location, and therefore the determination of the selection efficiency naturally accounts for the temporal inhomogeneity in sky coverage, as can be seen in Figure 1.

Using these parameters for each SN, rest-frame $UBVRI$ magnitudes are generated from the MLCS2k2 model for all dates on which the survey took data at the selected sky position. These magnitudes are modified according to the host galaxy extinction, K-corrected to the observed SDSS gri passbands, and further modified according to the estimated Milky Way extinction at that position (Schlegel et al. 1998). The zero-points from the survey are used to convert the gri magnitudes into flux values that would have been measured in ADUs by the SDSS 2.5 m telescope. The CCD gains are then used to determine the number of photo-electrons, and hence the signal and noise. Additional noise is computed for each measurement based on the measured observing conditions at each epoch, in each passband, at the assigned sky location. Sky noise is simulated by integrating the estimated sky noise per pixel over an effective aperture with a size determined by the local PSF estimate from `PHOTO`. Noise from the host galaxy is simulated by associating the SN with a host from the SDSS galaxy photometric redshift catalog (Oyaizu et al. 2007) selected to have a photometric redshift equal to the assigned SN redshift. In the SDSS DR5 (Adelman-McCarthy et al. 2007) `photoPrimary` database (Stoughton et al. 2002), each such galaxy image is fit with both an exponential and a de Vaucouleurs surface brightness profile. We use the exponential model in the r-band as a probability distribution from which the SN position within the galaxy is drawn. That is, the galaxy noise model assumes that the SN Ia rate is roughly proportional to r-band stellar luminosity. The estimated contribution of the galaxy light to the noise in each passband is computed by convolving the exponential galaxy model with the PSF in the survey image. In practice, this procedure is computationally expensive, so we pre-compute the noise values on a grid of model parameters and perform a multi-dimensional linear interpolation to obtain an estimate of the galaxy noise.

As a consistency check of the MC as a representation of the SN data, we compare the distributions of signal and noise in gri for the MC sample to the signal and noise for all photometric epochs for the low-redshift SNe Ia in the rate-measurement sample. The comparison of the distributions is shown in Fig. 9. The distributions of signal and noise are in good agreement, indicating that the MC model, and the assumed parameter distributions therein, provide a reasonable representation of the low-redshift SN Ia sample.

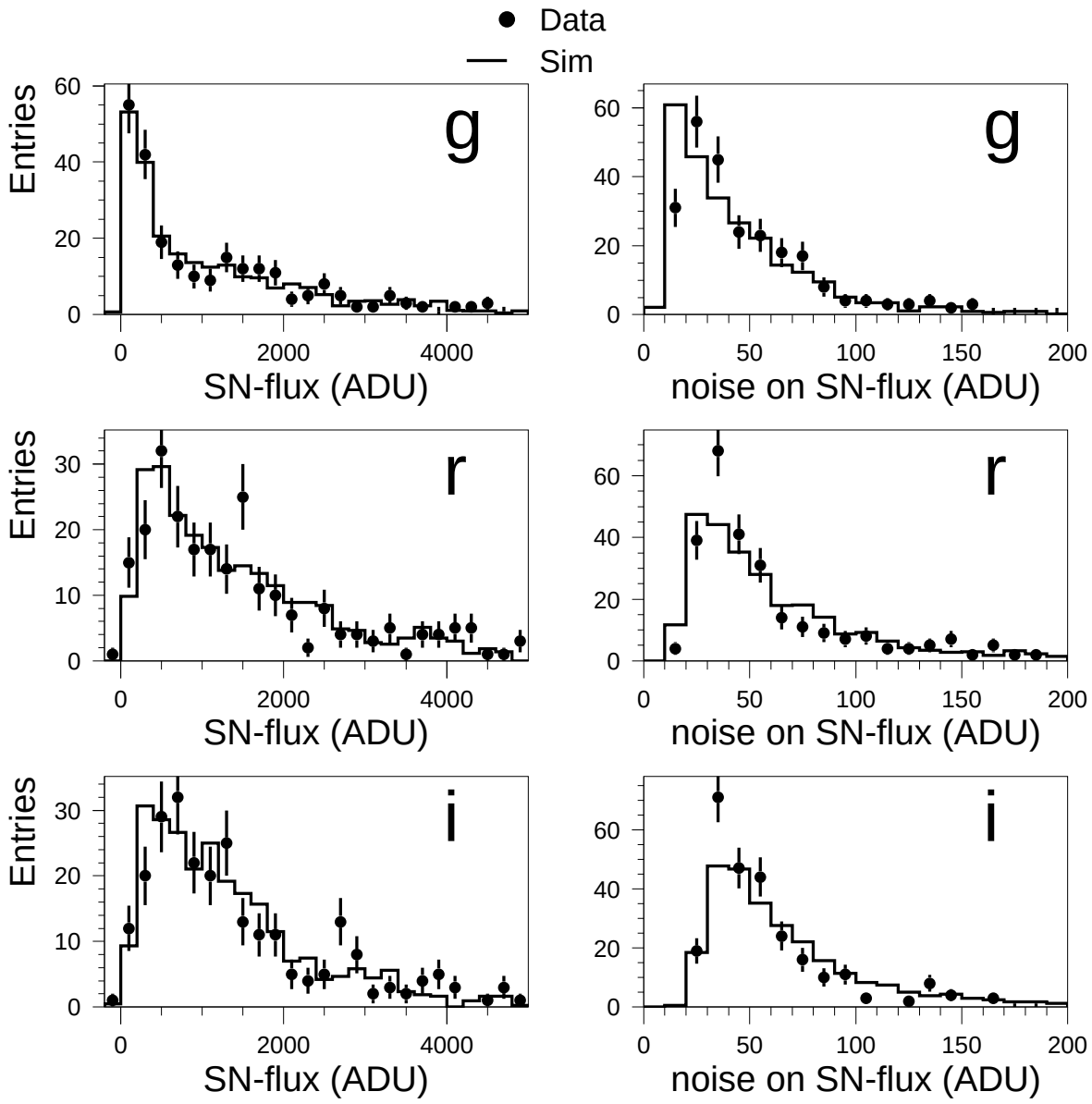

Fig. 9.— For SN Ia that satisfy the selection requirements (§3), the signal-flux and noise distributions are shown for all photometric epochs in the g,r,i filters. Each distribution is shown for SDSS data (dots) and for the simulation (histogram) that has been scaled to have the same number of entries as the data.

Having shown that the MC generates photometry that is consistent with our observed low-redshift SN Ia sample, we can use the MC to provide a more reliable determination of the detection efficiency of the on-mountain search pipeline than we could obtain with the relatively small number of low-redshift fakes. For each epoch generated by the MC, we use the efficiency as a function of signal-to-noise ratio in each passband (from Fig. 7) to determine the efficiency of the search pipeline to detect SNe Ia at all redshifts. The resulting software pipeline detection efficiency as a function of redshift, based on a MC study using 15640 total SNe (920 in each of 17 redshift bins) is shown in Figure 10; the efficiency is 100% over the redshift range $z \leq 0.12$. Since the fakes tests of §4.1 showed that the human scanning process causes a negligible loss of efficiency, we conclude that the combined efficiency for SN detection by the pipeline and identification as a candidate by humans is 100% over the redshift range of interest. This does not guarantee that the efficiency of the photometric typing code used for spectroscopic target selection (§2.2) is also 100%, but the studies of §3.2 indicate that, with the exception of SN 9266, there were no losses due to the target selection algorithm.

The final step is to use the MC to compute the survey discovery efficiency ϵ for a SN Ia sample defined by the selection requirements in §3.1. This efficiency is the ratio of the number of SNe Ia that are detected by the pipeline, identified by humans, and that pass the selection criteria of §3.1 to the total number of SNe Ia that reach peak light during the survey, i.e., between Sept. 1 and Nov. 30. While we have seen that the detection efficiency is essentially 100% out to $z = 0.12$, ϵ is less than 100% primarily because the selection requirements on light curve coverage (cuts 4 and 5 in §3.1) remove some SNe Ia that peaked in early September or late November. Using the MC sample of 15640 light-curves mentioned above and fitting a linear function to the resulting selection efficiency in the redshift range $0 < z < 0.12$ gives

$$\epsilon(z) = (0.78 \pm 0.01) + (-0.13 \pm 0.14)\ z \tag{1}$$

That is, the survey efficiency is approximately constant at low redshifts, changing by only $\sim 1\%$ over the redshift range of the rate measurement. The mean SN Ia discovery efficiency for our rate sample is $\langle\epsilon\rangle = 0.77 \pm 0.01$.

While the data-MC comparison in Fig. 9 indicates that we have made a consistent choice of the parameter distributions for the MC model, to estimate the systematic uncertainty in the discovery efficiency we vary the assumed MC parameter distributions and recompute the efficiency. We find that varying τ, the parameter controlling the extinction distribution, has the largest systematic effect on the determination of the discovery efficiency from the MC. Varying τ over the range $0.2-0.6$, the estimated discovery efficiency for the rate-measurement SN Ia sample changes by less than a percent.

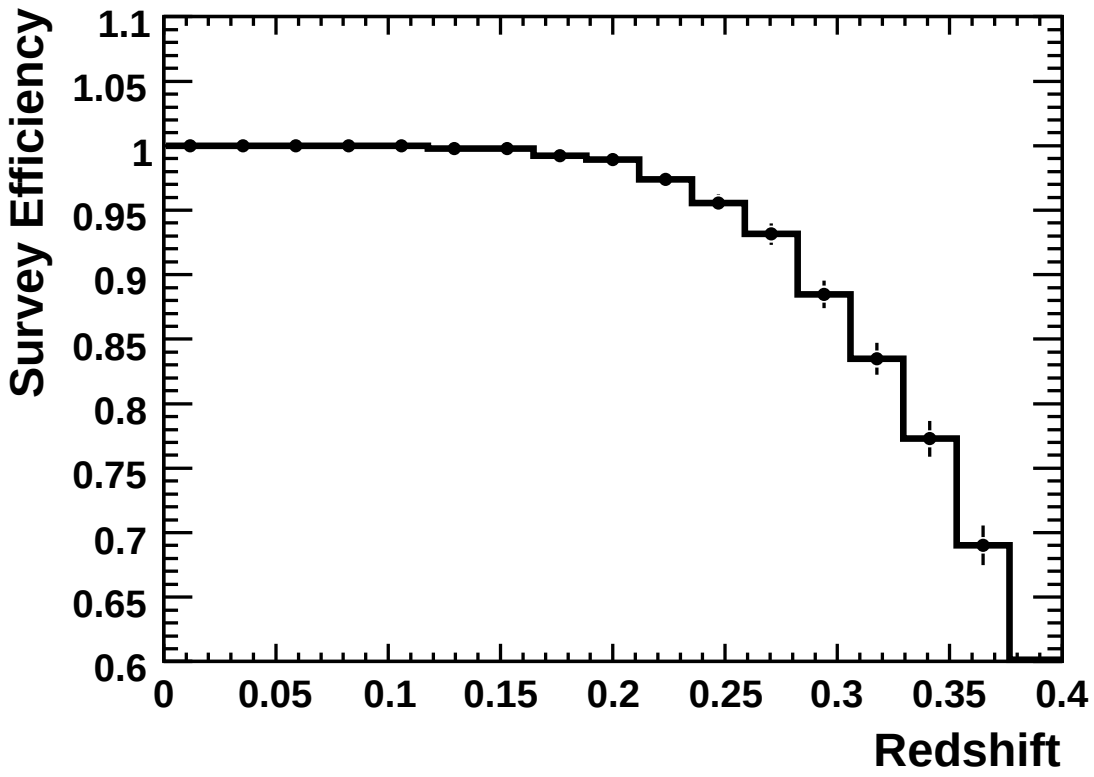

Fig. 10.— Search pipeline software efficiency as a function of SN Ia redshift, as determined from the Monte Carlo simulation.

5. SDSS SN Results

5.1. Volumetric SN Ia rate

For the purpose of interpreting the SN observations as a volumetric SN rate, we will assume a spatially flat cosmology with non-relativistic matter density $\Omega_m = 0.3$, dark energy density $\Omega_\Lambda = 0.7$, and dark energy equation of state parameter $w = p/\rho = -1$. For the low-redshift rate measurement presented in this section, the dependence on cosmological parameters of the survey selection efficiency is negligible, and so the uncertainty in the rate due to uncertainty in cosmology is due entirely to the difference in the volume of the survey. A change in Ω_m of 0.02 would lead to a 4% change in the rate measurement.

The observed volumetric SN rate, r_V, is defined as

$$r_V = \frac{N}{\widetilde{VT\epsilon}} \ , \tag{2}$$

where N is the number of SNe in the sample, and $\widetilde{VT\epsilon}$ is the effective product of the survey volume, V, the observer-frame survey duration, T, and the SN discovery efficiency, $\epsilon(z)$, estimated in §4.2,

$$\widetilde{VT\epsilon} = (\Theta T) \int_{z_{min}}^{z_{max}} dz \ \epsilon(z) u^2(z) \frac{du}{dz} \frac{1}{(1+z)} \ . \tag{3}$$

Here Θ is the solid angle covered by the survey and $u(z)$ is the comoving distance in the Friedmann-Robertson-Walker metric,

$$u(z) = \int_0^z \ dz' \frac{c}{H(z')} = \frac{c}{H_0} \int_0^z \frac{dz'}{\sqrt{\Omega_m (1+z')^3 + \Omega_\Lambda}} \ . \tag{4}$$

If the survey efficiency is independent of redshift, and if the redshift range covered by the SN observations is small, then $\widetilde{VT\epsilon} \sim (VT\epsilon)/(1 + \langle z \rangle)$, where V is the survey volume and $\langle z \rangle$ is the volume-weighted mean redshift of the survey.

For the SDSS-II Supernova Survey we have $N = 17$, $z_{min} = 0$, $z_{max} = 0.12$, $\langle \epsilon(z) \rangle = 0.77 \pm 0.01$, $T = 89$ days $= 0.244$ years, and $\Theta = 0.08277 * 0.98$ steradians. This value for Θ is 98% of the actual sky area covered by the survey, due to the masking of bright stars and variable sources. Substituting these values into Eqn. (2), we find a volumetric SN Ia rate of

$$r_V = [2.93^{+0.17}_{-0.04}(\text{systematic})^{+0.90}_{-0.71}(\text{statistical})] \times 10^{-5} \text{ SNe Mpc}^{-3}\ h_{70}^3 \text{ year}^{-1}\ , \qquad (5)$$

with $h_{70} \equiv H_0$ (70 km s^{-1}Mpc^{-1})$^{-1}$ and H_0 the present value of the Hubble parameter. The statistical errors quoted represent the standard frequentist 68.27% central confidence interval on the mean of a Poisson distribution. The systematic uncertainty represents uncertainty on our determination of the SN selection efficiency (§4.2) and on the number of photometrically identified SNe Ia (§3.2). This measurement represents the volume-averaged SN Ia rate at $z \leq 0.12$. When rate measurements are plotted vs. redshift, it is generally assumed that the rate is constant over the sampled redshift interval. If we assume that the SN Ia rate is constant at $z \leq 0.12$, then Eqn.(5) can be interpreted as the rate at the volume-weighted mean of our redshift range, $\langle z \rangle = 0.09$, and we make this assumption when plotting the result. Our result is shown along with previously reported SN Ia rate measurements in Fig. 11, but we defer discussion of comparison and combination with other measurements to §6.2.

5.2. SN Ia Rate per unit galaxy luminosity

Early measurements of the SN rate were generally derived from SN observations that targeted known galaxies; for these surveys, the SN rate is most naturally measured as a rate per unit luminosity in some passband, traditionally the B-band. Blanc et al. (2004) have converted a number of measurements from the literature of the SN Ia rate per unit luminosity to rates per unit volume, and in Table 4 we adopt their values for the Cappellaro et al. (1999); Madgwick et al. (2003); Hardin et al. (2000) rate measurements.

For completeness, we convert our volumetric rate to a rate per unit galaxy luminosity in the SDSS passbands. The galaxy luminosity functions in the SDSS passbands are estimated in Blanton et al. (2003). The corresponding luminosity densities in the *ugriz* passbands, at a mean redshift of $\langle z \rangle = 0.1$ are 1.60 ± 0.32, 1.25 ± 0.05, 1.29 ± 0.04, 1.48 ± 0.05, and 1.89 ± 0.05, in units of $10^8 L_\odot h_{70}$Mpc^{-3}, where $L_\odot$ is the solar luminosity. In combination with the volumetric rate measurement of Eqn.(5), this yields the SN Ia rate per unit luminosity in the SDSS passbands, $(r_L)_{ugriz}/h_{70}^2 = 0.183^{+0.06}_{-0.05}$ SNu$_u$, $0.235^{+0.07}_{-0.06}$ SNu$_g$, $0.227^{+0.07}_{-0.06}$ SNu$_r$, $0.197^{+0.06}_{-0.05}$ SNu$_i$, and $0.156^{+0.05}_{-0.04}$ SNu$_z$, where 1 SNu$_x \equiv 1$ SN $10^{-10} L_\odot^x$ (100 yr)$^{-1}$, with $L_\odot^x$ the luminosity in passband x, in units of solar luminosities.

5.3. SN Ia Rate as a function of host galaxy type

Recent measurements have shown that the specific SN Ia rate is higher in star-forming galaxies than in passive galaxies. For example, Mannucci et al. (2005) found that the SN Ia rate per unit stellar mass is $\sim 20-30$ times higher in late-type galaxies than in E/S0 galaxies. Sullivan et al. (2006) have found a similar trend in the SNLS data. We will consider the trend of SN rate vs. star formation activity using the SDSS-II Supernova Survey sample in a forthcoming publication.

Here, we consider the low-redshift SN Ia rate vs. host galaxy type. We have considered several photometric galaxy-type indicators that are accessible through the SDSS DR5 database (Adelman-McCarthy et al. 2007), including $u-r$ color (Strateva et al. 2001); the likelihood of the de Vaucouleurs model fit to the galaxy surface brightness profile relative to that of an exponential model fit; and the (inverse) concentration index (Shimasaku et al. 2001; Yamauchi et al. 2005), defined as the ratio of the radii that contain 50% and 90% of the Petrosian flux (see Stoughton et al. (2002) for definitions of these quantities). These parameters are listed in Table 3 for the host galaxies of the SNe included in the rate-measurement sample. Note that the $u-r$ color in Table 3 is computed using SDSS model magnitudes (Stoughton et al. 2002) and is *not* K-corrected to the galaxy restframe. A host galaxy is associated with each SN by determining the nearest object, based on a measure of the galaxy image size. Specifically, the SDSS DR5 catalog includes the parameters of an iso-photal ellipse for each galaxy-like object, and for each of the *ugriz* filter bands, defined as the ellipse where the object surface brightness is 25 magnitudes arcsec^{-2} (Stoughton et al. 2002). We define the distance to a potential host galaxy to be the semi-major axis of the ellipse that is similar (has the same aspect ratio and orientation) to the r-band iso-photal ellipse and that intersects with the position of the SN. The host galaxy for each SN is defined to be the nearest object in this measure. For the SNe listed in Table 1, the association of SN with host galaxy was confirmed through visual inspection of the images.

Early-type galaxies generally display red colors (large $u-r$), are reasonably well fit by a de Vaucouleurs surface brightness profile (large values of the relative de Vaucouleurs likelihood), and show relatively strong central light concentration (low values of the inverse concentration index). Consequently, these three indicators are strongly correlated and tend to give a consistent classification into early and late photometric types, indicated by the last column in Table 3. However, the classifications based on the three indicators do not always agree, in which case we have made a judgement based on visual inspection of the galaxy image and, where available, a high signal-to-noise galaxy spectrum. For these five cases, the host type indicated in the last column is marked with an asterisk.

Table 3. Host Galaxies for SNe Ia in the rate sample.

SDSS Id	α (J2000.0)	δ (J2000.0)	$u-r$	de Vaucouleurs likelihood	concentration index	Host Type
1241	22 30 41.15	−00 46 34.5	2.82	0.91	0.382	Early
1371	23 17 29.70	+00 25 46.8	2.97	0.00	0.377	Early*
2561	03 05 22.64	+00 51 35.0	2.59	0.00	0.410	Late*
3256	21 57 04.19	−00 13 24.5	1.99	0.00	0.442	Late
3592	01 16 12.71	+00 47 26.0	2.21	0.00	0.427	Late
3901	00 59 24.11	+00 00 09.5	1.40	1.00	0.418	Late*
5395	03 18 33.80	+00 07 24.0	1.29	0.49	0.360	Late*
5549	00 12 59.97	+00 14 54.9	1.01	0.46	0.461	Late
5944	01 56 48.50	−00 12 45.3	2.57	0.00	0.469	Early*
6057	03 30 12.89	−00 58 28.1	1.79	0.00	0.485	Late
6295	01 34 41.84	−00 36 15.2	2.97	1.00	0.312	Early
6558	01 26 48.46	−01 14 17.3	2.23	0.00	0.427	Late
6962	02 35 26.58	+01 04 28.3	2.71	1.00	0.379	Early
7147	23 20 04.44	−00 03 20.2	3.22	1.00	0.350	Early
7876	01 16 43.87	+00 47 36.9	1.71	0.00	0.532	Late
8719	00 30 53.23	−00 43 07.3	1.12	0.01	0.412	Late
9266	03 20 43.19	−01 00 08.2	2.25	0.00	0.398	Late

*At least one of the three photometric type indicators indicates a different type from that listed.

Note. — SDSS Id denotes internal candidate designation. α and δ are the coordinates of the host galaxy of the SN. The photometric morphology indicators, $u-r$, de Vaucouleurs likelihood, and concentration index are described in (§5.3).

Of the three photometric type indicators, $u-r$ correlates most strongly with the host type we have assigned to each galaxy in the last column of Table 3. The distribution of SDSS galaxies is approximately bimodal in $u-r$ (Strateva et al. 2001), suggesting a natural division between early and late types. We therefore use $u-r$ as the galaxy classifier for the purpose of studying the SN rate vs. galaxy type. This is preferable to using the 'host type' classification in Table 3, since the subjective human judgement required to determine the latter makes it difficult to determine its population properties. Strateva et al. (2001) suggest that $u-r=2.2$ is an optimal separator between early and late types. However, our catalog of galaxies with photometric redshifts in stripe 82 (Oyaizu et al. 2007) appears to be better separated into two subpopulations using $u-r=2.4$. Since a division at $u-r=2.4$ also provides better agreement with the subjective 'host type' classification in Table 3, we use this color cut to separate the hosts into early ($u-r>2.4$) and late ($u-r<2.4$) types for the relative rate measurement. Using a large sample of galaxies from the SDSS DR5 database, we find that the fractional r-band luminosity densities for early and late-type galaxies at redshifts $z\leq 0.12$ are 54% and 46%, respectively. From Table 3, we find that the SN Ia rate per unit r-band luminosity is $\sim 1.68^{+0.52}_{-0.41}$ times higher in late-type galaxies than in early-type galaxies. Using the luminosity functions of Blanton et al. (2003), we find that the absolute rates per unit luminosity are $r_L/h_{70}^2 = 0.085^{+0.03}_{-0.02}$ SNu_r (early) and $0.142^{+0.04}_{-0.03}$ SNu_r (late). The evidence for a larger SN Ia rate in late-type galaxies is statistically marginal with the current low-redshift sample. The systematic uncertainty is also significant: if we place the host galaxy type cut at $u-r=2.2$, we find no significant difference between the rate per unit luminosity in early- and late-type hosts.

6. Fitting SN Rate evolution models

As noted in §1, models for SN Ia progenitors in principle can be distinguished by their predictions for the evolution of the SN Ia rate with cosmic time. In this section, we present a general maximum likelihood method of fitting SN observations to models with a redshift-dependent SN rate. We then apply the method to a recently discussed SN Ia rate model, using data from the SDSS-II Supernova Survey and from other published rate measurements.

6.1. Maximum Likelihood method

In this section we describe a method for fitting SN data to models of the SN rate without binning the data. The method is similar to the methods described in Strolger et al. (2004). and Strolger & Riess (2006). A distinguishing feature of our analysis is that it allows for

combining multiple data sets and accounts for systematic errors.

A general model for the volumetric SN rate can be written as $r_V(z;\mathbf{p})$, where $\mathbf{p}$ represents the set of model parameters. According to the model, the total number of detected SNe follows a Poisson distribution with mean value

$$\langle N(\mathbf{p})\rangle = \int_0^\infty dz\ \Theta T\epsilon(z)\ \frac{r_V(z;\mathbf{p})}{(1+z)}\ u^2(z)\ \frac{du}{dz}\ , \tag{6}$$

where all symbols were defined in §5. The probability of detecting a SN at redshift z is given by the integrand of Eqn.(6), $P(z_i) \propto d\langle N(\mathbf{p})\rangle/dz$, giving a likelihood function for detecting SNe at the N observed redshifts $\{z_i\}$,

$$L(\{z_i\};\mathbf{p}) = \frac{e^{-\langle N(\mathbf{p})\rangle}\langle N(\mathbf{p})\rangle^N}{N!}\prod_{i=1}^{N}\frac{1}{\langle N(\mathbf{p})\rangle}\frac{d\langle N(\mathbf{p})\rangle}{dz}. \tag{7}$$

The corresponding log-likelihood function, suppressing terms that do not depend on the model parameters, is

$$\log L(\{z_i\};\mathbf{p}) = -\langle N(\mathbf{p})\rangle + \sum_{i=1}^{N}\log\left(\Theta T\epsilon(z_i)\ \frac{r_V(z_i;\mathbf{p})}{(1+z_i)}\ u^2(z_i)\left[\frac{du}{dz}\right]_{z_i}\right)\ . \tag{8}$$

The best-fit model is determined by maximizing the log-likelihood with respect to the model parameters, $\mathbf{p}$. To incorporate information about the systematic error in our fits, we weight the contribution to the log-likelihood for each data set by multiplying each term in the log-likelihood function by the factor $\sigma_{stat}^2/(\sigma_{stat}^2+\sigma_{syst}^2)$, where σ_{stat} and σ_{syst} are the statistical and systematic errors for the measurement. This factor assumes that the systematic errors are approximately Gaussian and independent of the statistical errors. We note that auxiliary information about the model parameters and uncertainties in the survey parameters Θ, T, and $\epsilon(z)$ could be incorporated in a more rigorous way via prior probability distributions. However, this would require full knowledge of the probability distribution functions for the efficiency, subject to all possible variations of systematic effects, which is in practice unknown.

To combine data from multiple surveys, the log-likelihood functions for each survey are added together, using the appropriate values of $\epsilon(z)$, Θ, and T for each survey. The advantage of this method is that it does not involve binning the SN data in redshift; however, it does require knowledge of the efficiency function $\epsilon(z)$ for each survey. To evaluate the goodness of fit of a given model, one can use, e.g., the Kolmogorov-Smirnov (KS) test applied to the data and to a large-statistics Monte Carlo sample generated from the best-fit model parameters.

The code for fitting rate models was tested on large MC samples (~ 1000 SNe), and the MC model parameters were accurately recovered.

As an illustration of the likelihood method, we apply it to the SDSS-II Supernova Survey data, assuming a redshift-independent model over the redshift range probed by the data, $r_V(z) =$ constant. In this case, the rate that maximizes the likelihood can be shown analytically to be given by Eqn. 2. The probability for this model from the KS test statistic is $p_{KS} = 0.42$, meaning that if the model is correct, 42% of sample observations drawn from the model would have a KS test statistic as large or larger than that found in comparing this data set to the model. In the discussion that follows the probabilities from the KS test are given as rough estimators of the goodness of fit only; the distribution of the KS test statistic does not in general have an analytic form when model parameters are estimated from the data.

6.2. SN Rate Models and Star Formation History

As discussed in §1, measurements of the SN Ia rate provide a means to distinguish between models of SN Ia progenitor systems. The connection between the observed SN Ia rate and the progenitor systems is made through the relation of the SN rate to the cosmic star formation history. Sometime after a population of stars form, a fraction of them will end up in binary systems that are producing SN Ia explosions. If we denote the distribution of delay times between formation of the progenitor systems and the SN explosions by $D(t)$, then the volumetric SN Ia rate $r_V(t)$ and the cosmic star formation rate $\dot{\rho}(t)$ are related by

$$r_V(t) = \int_0^t dt' \dot{\rho}(t') D(t - t') \ . \tag{9}$$

We can therefore constrain models for the distribution of delay times, $D(t)$, by comparing the SN Ia rate and the star formation rate. A discussion of predicted delay-time distributions for a variety of SN Ia progenitor models is given in Greggio (2005). A simple model distribution that allows for two distinct contributions to the SN Ia rate is

$$D(t) = A + B\delta(t) \tag{10}$$

where $\delta(t)$ is the Dirac delta function. This '$A + B$' model was proposed by Mannucci et al. (2006) and Scannapieco & Bildsten (2005) and it has been used in SN rate studies by the SNLS (Neill et al. 2006) and Sullivan et al. (2006). The SN rate can be written $r_V(t) =$

$A\rho(t)+B\dot{\rho}(t)$, where $\rho(t)$ is the stellar mass density. The B term represents an instantaneous or prompt SN Ia component and the A term represents an extended component in which SNe Ia form with uniform probability in the time interval following star formation. In addition to the '$A+B$' model, we also consider a simple model in which $r_V(t)$ evolves as a power law in redshift, independent of considerations of star formation history.

6.3. Rate Measurements: Combining Data Sets

The constraints on redshift-dependent models of the SN Ia rate are improved if one uses SN observations over a wide range of redshifts. In the following, we combine the low-redshift rate measurement from the SDSS-II Supernova Survey with other SN Ia rate measurements in the literature. For each data set, we require both the SN redshifts and an estimate of the redshift-dependent selection function $\epsilon(z)$, and we therefore restrict ourselves to using data sets for which it is straightforward to infer the redshift dependence of the efficiency. We note that several authors, including Barris & Tonry (2006) and Poznanski et al. (2007) have made SN rate measurements based on samples of photometrically identified SNe. However, in combining data sets for the present analysis, we will restrict ourselves to rate measurements that are based primarily on spectroscopically identified SNe. Of the nine previously published rate measurements that have been based on primarily spectroscopically identified SNe, shown in Fig. 11, we will make use of four, in addition to the one in this work. These five rate measurements are shown in bold font in Table 4. The weighting factors, used to account for the systematic uncertainty on each measurement, are listed in the last column of Table 4. In cases where the uncertainty on the measurement is asymmetric, we define the weighting factor to be the mean of the upper and lower weighting factors. Varying the weighting factor between the extremes of using the smaller weight, and of using the larger weight, the best-fit parameters change by $\sim 5\%$ of the statistical error. In the subsections below, we briefly describe the data from other measurements that we include in the model fits and how we describe their efficiency function. We also discuss measurements that we exclude from the model fits.

Table 4. SN Ia Rate Measurements.

Reference	Redshift Range	Mean Redshift	N_{SNe}	Rate $[10^{-5}$ SNe h_{70}^3 Mpc^{-3} yr$^{-1}]$	$\sigma_{stat}^2/\sigma_{tot}^2$
Cappellaro et al. (1999)*	~ 0	~ 0	70	2.8 ± 0.9	N/A
This work*	$0 - 0.12$	0.09	17	$2.9^{+0.9}_{-0.7}$	0.988
Madgwick et al. (2003)	$0 - 0.19$	0.10	19	3.1 ± 1.6	N/A
Blanc et al. (2004)	$0 - 0.3$	0.13	14	$2.0^{+0.84}_{-0.72}$	N/A
Hardin et al. (2000)	$\sim 0.02 - 0.2$	0.14	4	$3.4^{+2.9}_{-1.7}$	N/A
Dahlen et al. (2004)	$0.2 - 0.6$	0.45	3	$6.9^{+15.8}_{-3.7}$	N/A
Neill et al. (2006)*	$0.2 - 0.6$	0.45	73	$4.2^{+1.4}_{-1.1}$	0.492
Tonry et al. (2003)	$\sim 0.25 - 0.6$	0.46	8	4.8 ± 1.7	N/A
Pain et al. (2002)*[a]	$0.25 - 0.85$	0.55	37	$5.4^{+1.5}_{-1.4}$	0.643
Dahlen et al. (2004)*	$1.0 - 1.4$	1.2	6	$11.5^{+4.7}_{-5.1}$	0.686

[a]The value of the rate has been corrected to our assumed cosmology, according to equation 3 of Pain et al. (2002).

Note. — Measurements included in the model fits are shown in bold face, and are marked with an asterisk. Mean redshift refers to the mean of the expected SN redshift distribution, under the assumption of a constant SN rate. For Madgwick et al. (2003), this is estimated as the mean of the observed SN redshift distribution. Systematic and statistical errors, when reported separately, have been combined in quadrature. Rate measurements reported here assume constant volumetric rate over the range of each survey. σ_{stat} is the reported statistical error on the measurement. σ_{tot} is the sum in quadrature of the reported statistical and systematic errors.

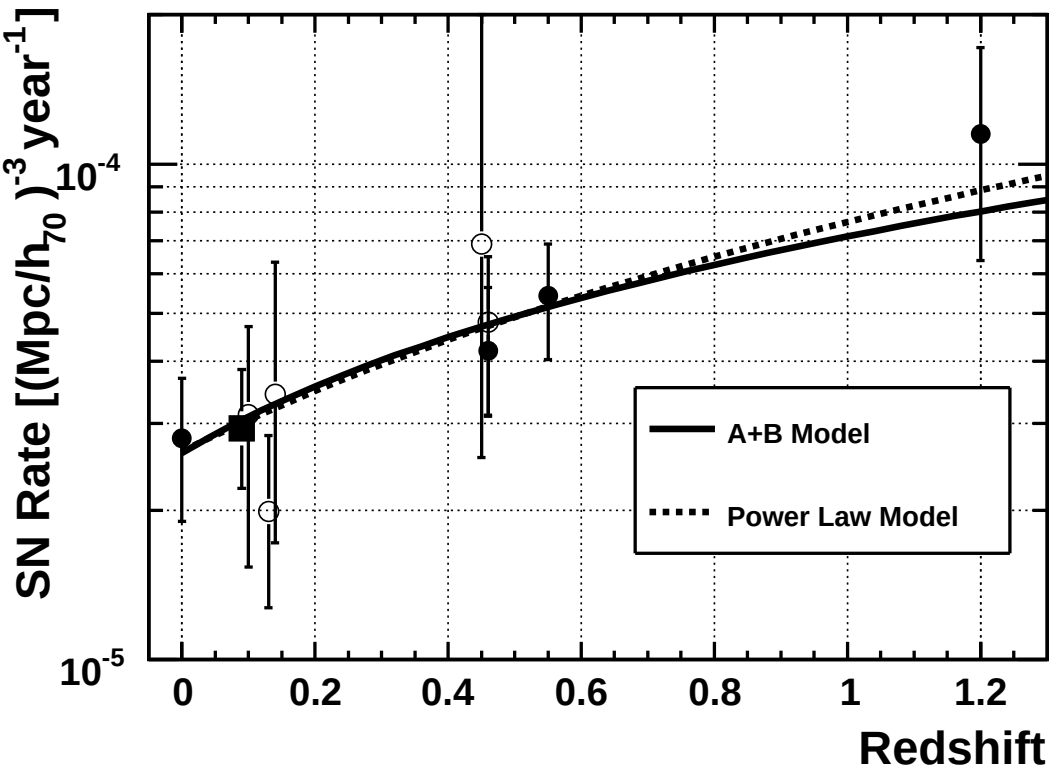

Fig. 11.— Measurements of the SN Ia rate discussed in §6.3. The SDSS-II Supernova Survey measurement in this paper is shown as the solid black square. Measurements for which the data is used in the model fits are shown as solid circles (see Table 4), and measurements not used in the fits as open circles. To plot each measurement, we have assumed in each case a model in which the rate is constant over the redshift range covered by that measurement. The rate as a function of redshift for the best fitting '$A + B$' and power law models are overlaid.

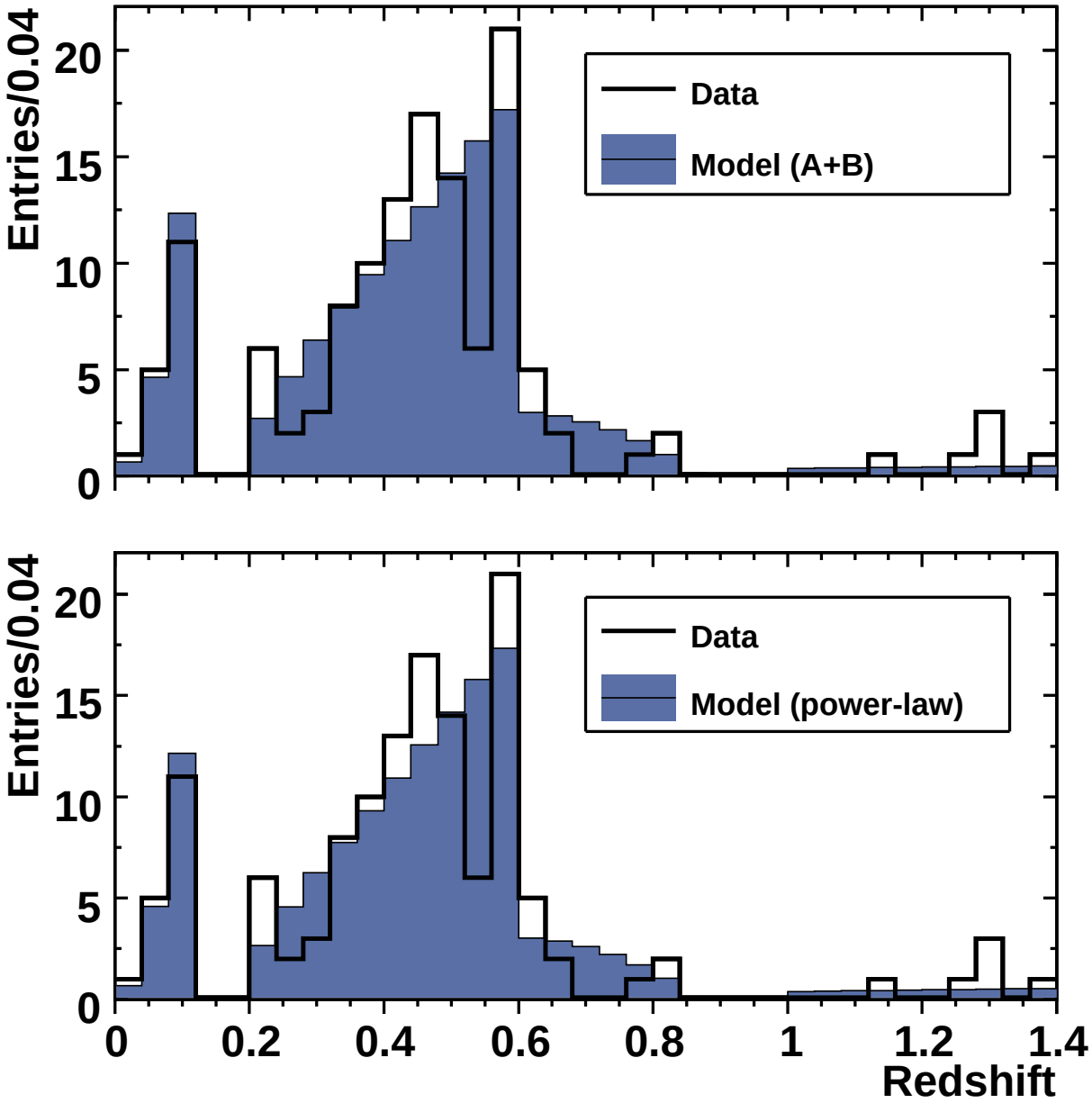

Fig. 12.— Comparison of the observed distribution of SNe and the predicted distributions for the $A + B$ and power law rate models. In each panel the shaded region shows the predicted redshift distribution of the best-fit model. The figures include the five highlighted data sets in Table 4.

6.3.1. Other rate measurement data included in the model fits

Neill et al. (2006) measured the SN Ia rate using 73 SNe Ia from the SNLS. They state that their sample is spectroscopically complete, i.e., that $\epsilon(z)$ is constant, to $z = 0.6$. Including the solid-angle and survey observation time, the factor $\Theta T\epsilon(z) = 7.37 \times 10^{-4}$ steradian year.

The measurement of Pain et al. (2002) is based on data from the Supernova Cosmology Project, covering about 12 square degrees. Although Pain et al. (2002) do not give $\epsilon(z)$ explicitly, they do provide the redshift distribution of SNe recovered from their Monte Carlo simulations which assumed a constant rate per unit comoving volume. With this information, we can compute the relative number of MC-generated SNe in each redshift bin and thereby the redshift dependence of their efficiency function. Fitting a quadratic function to this tabulated efficiency function in the range $0.25 < z < 0.85$ gives $\Theta T\epsilon(z) = (2.68 + 0.61z - 4.22z^2) \times 10^{-4}$ steradian year.

Cappellaro et al. (1999) measured the SN Ia rate for the local Universe by combining data from a number of surveys, including visual searches of nearby galaxies. Although they do not provide an efficiency function or a redshift distribution, the redshift range covered by the measurement is so small that we take the quoted result to be the SN Ia rate at $z = 0$. We include the Cappellaro et al. (1999) rate measurement by adding a standard χ^2 term to the log-likelihood function, i.e., a term of the form $(r_V(0;\mathbf{p}) - r_{V,Capp})^2/2\sigma^2_{Capp}$, where $r_V(0;\mathbf{p})$ is the model prediction at redshift zero, $r_{V,Capp}$ is the Cappellaro et al. (1999) measurement in Table 4, and σ_{Capp} is the quoted error on the measurement.

Dahlen et al. (2004) measured the SN Ia rate to $z \sim 1.6$ using data from the Great Observatories Origins Deep Survey (GOODS) carried out with the Advanced Camera for Surveys on the Hubble Space Telescope (HST). [4] We use their measurement in the redshift range $1.0 < z < 1.4$. Using their scaled efficiency function, as inferred from Figure 14 of Strolger et al. (2004), we fit a function $A + Bz + Cz^2 + Dz^3$, valid in the redshift range $1.0 < z < 2.0$. The best-fit parameters are $A = -7.557, B = 55.93, C = -51.07$ and $D = 12.5$. This function is normalized so that the number of expected SNe for their survey is equal to six, the number they observed in the redshift interval $1.0 < z < 1.4$, giving a value of $\Theta T\epsilon(z) = [-10.35 + 76.61z - 69.95z^2 + 17.12z^3] \times 10^{-4}$ steradian year.

The redshift dependence of the efficiency function for the present data set is discussed in §4.2; including the solid-angle and survey observation time, $\Theta T\epsilon(z) = [1.54 - 0.025z] \times 10^{-2}$

[4]Just before we submitted this paper, Kuznetsova et al. (2007) released new SN Ia rate measurements based on analysis of 57 SNe from HST, including the 42 SNe analyzed by Dahlen et al. (2004).

steradian year.

6.3.2. Rate measurement data not included in the fits

In fitting the models, we choose not to include several of the SN Ia rate measurements listed in Table 4. We exclude the Dahlen et al. (2004) rate measurement in the redshift range $0.2 < z < 0.6$ because the efficiency function, given by Strolger et al. (2004), is only plotted for redshifts greater than 1, and because the 73 SNe from SNLS (Neill et al. 2006) in the same redshift range dominate the fit in comparison to the 3 SNe from Dahlen et al. (2004). Similar reasoning holds for the measurement of Tonry et al. (2003), which is based on 8 SNe in the redshift range well covered by the SNLS, and for which the redshifts are not explicitly stated. Both the Hardin et al. (2000) and the Blanc et al. (2004) rate measurements, based on data from the EROS microlensing survey, included a requirement that each SN be associated with a host galaxy with apparent magnitude $R \lesssim 19$, which introduces a bias against faint hosts. If SNe Ia occurred at a constant rate per unit R-band luminosity in all galaxies, this would not be an issue. However, as noted above, it has been shown that the SN Ia rate per unit stellar mass (for which the total R-band luminosity is a proxy) is a function of SFR (Mannucci et al. 2005; Sullivan et al. 2006). Finally, the Madgwick et al. (2003) measurement is based on SNe discovered via principal component analysis in spectra obtained by the SDSS galaxy redshift survey. This measurement has significant systematic uncertainties that are different from those in photometric surveys. In particular, the SNe discovered by this technique must lie within approximately 1.5" of the cores of their host galaxies, the radius of the SDSS spectroscopic fibers. To derive a SN rate from these spectroscopic observations, assumptions are needed about how SNe are distributed within their host galaxies at larger galactocentric distances.

6.4. Fits to SN Ia Rate Models

We now consider fits of the combined SN Ia rate measurements to the rate models discussed in §6.2, using the maximum likelihood approach of §6.1. The errors quoted below are the values of the fit parameters for which the log-likelihood function changes by 1/2 compared to its maximum, which assumes that the likelihood function is approximately Gaussian. We use the MINUIT software package (James & Roos 1994) for the function optimization and error analysis.

6.4.1. *Power-law redshift evolution of r_V*

We first consider a simple two-parameter model that describes power-law redshift evolution of the SN rate independent of consideration of the star formation history, $r_V(z) = \alpha(1+z)^{\beta}$. The best-fit power-law model is shown as the dashed curve in Fig. 11, and the predicted redshift distribution is shown in Fig. 12. Fitting this model to the five data sets, we find

$$\begin{aligned} \alpha &= (2.6^{+0.6}_{-0.5}) \times 10^{-5} \text{ SNe Mpc}^{-3} \text{ h}^3_{70} \text{ yr}^{-1} \\ \beta &= (1.5 \pm 0.6) \\ \rho_{\alpha\beta} &= -0.80 \end{aligned}$$

where $\rho_{\alpha\beta}$ is the correlation coefficient between the two fitted parameters. The KS probability for this model is $p_{KS} = 0.63$. We emphasize that the fitted value of β is greater than 0, i.e., the rate is determined to be an increasing function of redshift, at the $\sim 2.5\sigma$ level.

6.4.2. *The 'A+B' model*

We next consider the '$A + B$' model, with $D(t)$ given by Eqn. 10. As discussed by Förster et al. (2006), there is still significant uncertainty on the cosmic star formation rate (SFR), which is a limitation for placing observational constraints on SN delay time models. In what follows we choose one estimate of the SFR, and do not propagate the systematic uncertainties in the SFR. We follow the approach of Neill et al. (2006) and take the star formation rate from Hopkins & Beacom (2006). The functional form of the star formation rate is

$$\dot{\rho}(z) = \frac{a + bz}{1 + (z/c)^d} \; h_{100} \text{ M}_{\odot} \text{ yr}^{-1} \text{ Mpc}^{-3} \; , \tag{11}$$

where $h_{100} = H_0$ (100 km sec^{-1} Mpc^{-1})$^{-1}$, $a = 0.0118, b = 0.08, c = 3.3$, and $d = 5.2$. For the stellar mass density (the A component) we integrate the star formation rate over time; as mentioned by Neill et al. (2006), this can be expected to overestimate the total stellar mass density relative to estimates of the stellar mass density that are based on luminosity, as it includes a contribution from stars that have burned out. Performing the fit using the five data sets gives

$$\begin{aligned} A &= (2.8 \pm 1.2) \times 10^{-14} \text{ SNe M}_{\odot}^{-1} \text{ yr}^{-1} \\ B &= (9.3^{+3.4}_{-3.1}) \times 10^{-4} \text{ SNe M}_{\odot}^{-1} \\ \rho_{AB} &= -0.78 \end{aligned}$$

where ρ_{AB} is the correlation coefficient between the two fitted parameters. The KS probability for this model is $p_{KS} = 0.71$. The best-fit '$A + B$' model is shown as the solid curve in Fig. 11, and the predicted redshift distribution is shown in Fig. 12. We note that the uncertainties on the A and B parameters are $\sim 43\%$ and $\sim 35\%$, respectively. For comparison, if we perform a fit to the '$A + B$' model, suppressing the SDSS data, the uncertainties on the fit parameters are $\sim 53\%$ and $\sim 38\%$, respectively. Our analysis here is similar to that presented by Neill et al. (2006), with the primary differences being that we use a different subset of the available data, and we use a maximum likelihood method to fit the data to models of the SN rate. For comparison, Neill et al. (2006) found values of $A = (1.4 \pm 1.0) \times 10^{-14}$ SNe $M_{\odot}^{-1}$ yr^{-1} and $B = (8.0 \pm 2.6) \times 10^{-4}$ SNe $M_{\odot}^{-1}$. Both analyses find evidence for two components to the SN rate with the significance of the 'A' (extended) component less than that of the 'B' (prompt) component.

We note that one cannot accurately judge the goodness of fit of this model using a visual inspection or χ^2 fit to Fig. 11, since the measurements are each plotted *assuming* a constant-rate model. A better picture of the goodness of fit is given by Fig. 12, which shows the observed redshift distribution for the five data sets compared with the predicted redshift distributions for the '$A+B$' and power-law rate models convolved with the measured efficiency functions for the different measurements. The agreement between the predicted distributions for both evolving models and that of the data is quite reasonable.

7. Conclusions

We have presented a measurement of the SN Ia rate in the redshift range $0 < z \leq 0.12$ from the first season of the SDSS-II Supernova Survey. After selection cuts, the rate-measurement sample includes a total of 17 SNe Ia, of which 16 were spectroscopically confirmed. The final SN in the sample is a highly extincted, photometrically identified SN Ia with a measured host galaxy redshift. The insertion of artificial SNe in the data stream and the use of detailed Monte Carlo simulations of the survey efficiency, along with the rolling nature of the SDSS-II Supernova Survey, have enabled us to obtain a SN Ia rate measurement with smaller systematic uncertainties than previous measurements in a comparable redshift range.

We have also applied a maximum-likelihood technique, which enables us to account for systematic errors and to fit multiple SN data sets to models of the SN rate as a function of redshift. This maximum likelihood method makes optimal use of the available data, but requires estimates of the SN detection efficiency, and its uncertainty, as a function of redshift. We have applied this technique to a combination of recent SN Ia data sets, focusing on the

'$A + B$' model that relates the SN Ia rate to the cosmic star formation rate.

Models in which the SN Ia rate evolves with redshift are preferred over a model with a constant rate, but the data do not distinguish significantly between a simple power-law evolution of the SN Ia rate with redshift and the '$A + B$' model. The A and B parameter values we obtain are in good agreement with the results of Neill et al. (2006).

In the near future, we will use SDSS-II Supernova Survey data to extend this study in several directions, including a higher-statistics measurement of the low-redshift rate, measurement of the SN Ia rate vs. host galaxy star-formation rate and other host galaxy properties, and measurement of the SN Ia rate to $z \sim 0.3$. The Fall 2006 and Fall 2007 observing seasons each yielded ~ 30 spectroscopically confirmed SNe Ia at redshift $z \leq 0.12$, comparable to the size of the 2005 data set analyzed here. The final SDSS-II Supernova Survey sample includes of order 500 spectroscopically confirmed SNe Ia to $z < 0.4$.

Funding for the SDSS and SDSS-II has been provided by the Alfred P. Sloan Foundation, the Participating Institutions, the National Science Foundation, the U.S. Department of Energy, the National Aeronautics and Space Administration, the Japanese Monbukagakusho, the Max Planck Society, and the Higher Education Funding Council for England. The SDSS Web Site is http://www.sdss.org/.

The SDSS is managed by the Astrophysical Research Consortium for the Participating Institutions. The Participating Institutions are the American Museum of Natural History, Astrophysical Institute Potsdam, University of Basel, University of Cambridge, Case Western Reserve University, University of Chicago, Drexel University, Fermilab, the Institute for Advanced Study, the Japan Participation Group, Johns Hopkins University, the Joint Institute for Nuclear Astrophysics, the Kavli Institute for Particle Astrophysics and Cosmology, the Korean Scientist Group, the Chinese Academy of Sciences (LAMOST), Los Alamos National Laboratory, the Max-Planck-Institute for Astronomy (MPIA), the Max-Planck-Institute for Astrophysics (MPA), New Mexico State University, Ohio State University, University of Pittsburgh, University of Portsmouth, Princeton University, the United States Naval Observatory, and the University of Washington.

This work is based in part on observations made at the following telescopes. The Hobby-Eberly Telescope (HET) is a joint project of the University of Texas at Austin, the Pennsylvania State University, Stanford University, Ludwig-Maximillians-Universität München, and Georg-August-Universität Göttingen. The HET is named in honor of its principal benefactors, William P. Hobby and Robert E. Eberly. The Marcario Low-Resolution Spectrograph is named for Mike Marcario of High Lonesome Optics, who fabricated several optical elements for the instrument but died before its completion; it is a joint project of the Hobby-Eberly

Telescope partnership and the Instituto de Astronomía de la Universidad Nacional Autónoma de México. The Apache Point Observatory 3.5 m telescope is owned and operated by the Astrophysical Research Consortium. We thank the observatory director, Suzanne Hawley, and site manager, Bruce Gillespie, for their support of this project. The Subaru Telescope is operated by the National Astronomical Observatory of Japan. The William Herschel Telescope is operated by the Isaac Newton Group, on the island of La Palma in the Spanish Observatorio del Roque de los Muchachos of the Instituto de Astrofisica de Canarias. Kitt Peak National Observatory, National Optical Astronomy Observatory, is operated by the Association of Universities for Research in Astronomy, Inc. (AURA) under cooperative agreement with the National Science Foundation.

This work was supported in part by the Kavli Institute for Cosmological Physics at the University of Chicago through grants NSF PHY-0114422 and NSF PHY-0551142 and an endowment from the Kavli Foundation and its founder Fred Kavli.

REFERENCES

Adelman-McCarthy, J. K., Agüeros, M. A., Allam, S. S., Anderson, K. S. J., Anderson, S. F., Annis, J., Bahcall, N. A., Bailer-Jones, C. A. L., Baldry, I. K., Barentine, J. C., Beers, T. C., Belokurov, V., Berlind, A., Bernardi, M., Blanton, M. R., Bochanski, J. J., Boroski, W. N., Bramich, D. M., Brewington, H. J., Brinchmann, J., Brinkmann, J., Brunner, R. J., Budavári, T., Carey, L. N., Carliles, S., Carr, M. A., Castander, F. J., Connolly, A. J., Cool, R. J., Cunha, C. E., Csabai, I., Dalcanton, J. J., Doi, M., Eisenstein, D. J., Evans, M. L., Evans, N. W., Fan, X., Finkbeiner, D. P., Friedman, S. D., Frieman, J. A., Fukugita, M., Gillespie, B., Gilmore, G., Glazebrook, K., Gray, J., Grebel, E. K., Gunn, J. E., de Haas, E., Hall, P. B., Harvanek, M., Hawley, S. L., Hayes, J., Heckman, T. M., Hendry, J. S., Hennessy, G. S., Hindsley, R. B., Hirata, C. M., Hogan, C. J., Hogg, D. W., Holtzman, J. A., Ichikawa, S.-i., Ichikawa, T., Ivezić, Ž., Jester, S., Johnston, D. E., Jorgensen, A. M., Jurić, M., Kauffmann, G., Kent, S. M., Kleinman, S. J., Knapp, G. R., Kniazev, A. Y., Kron, R. G., Krzesinski, J., Kuropatkin, N., Lamb, D. Q., Lampeitl, H., Lee, B. C., Leger, R. F., Lima, M., Lin, H., Long, D. C., Loveday, J., Lupton, R. H., Mandelbaum, R., Margon, B., Martínez-Delgado, D., Matsubara, T., McGehee, P. M., McKay, T. A., Meiksin, A., Munn, J. A., Nakajima, R., Nash, T., Neilsen, Jr., E. H., Newberg, H. J., Nichol, R. C., Nieto-Santisteban, M., Nitta, A., Oyaizu, H., Okamura, S., Ostriker, J. P., Padmanabhan, N., Park, C., Peoples, J. J., Pier, J. R., Pope, A. C., Pourbaix, D., Quinn, T. R., Raddick, M. J., Re Fiorentin, P., Richards, G. T., Richmond, M. W., Rix, H.-W., Rockosi, C. M., Schlegel, D. J., Schneider, D. P., Scranton, R., Seljak,

U., Sheldon, E., Shimasaku, K., Silvestri, N. M., Smith, J. A., Smolčić, V., Snedden, S. A., Stebbins, A., Stoughton, C., Strauss, M. A., SubbaRao, M., Suto, Y., Szalay, A. S., Szapudi, I., Szkody, P., Tegmark, M., Thakar, A. R., Tremonti, C. A., Tucker, D. L., Uomoto, A., Vanden Berk, D. E., Vandenberg, J., Vidrih, S., Vogeley, M. S., Voges, W., Vogt, N. P., Weinberg, D. H., West, A. A., White, S. D. M., Wilhite, B., Yanny, B., Yocum, D. R., York, D. G., Zehavi, I., Zibetti, S., & Zucker, D. B. 2007, ApJS, 172, 634

Alard, C. & Lupton, R. H. 1998, ApJ, 503, 325

Aldering, G., Antilogus, P., Bailey, S., Baltay, C., Bauer, A., Blanc, N., Bongard, S., Copin, Y., Gangler, E., Gilles, S., Kessler, R., Kocevski, D., Lee, B. C., Loken, S., Nugent, P., Pain, R., Pécontal, E., Pereira, R., Perlmutter, S., Rabinowitz, D., Rigaudier, G., Scalzo, R., Smadja, G., Thomas, R. C., Wang, L., & Weaver, B. A. 2006, ApJ, 650, 510

Barris, B. J. & Tonry, J. L. 2006, ApJ, 637, 427

Blanc, G., Afonso, C., Alard, C., Albert, J. N., Aldering, G., Amadon, A., Andersen, J., Ansari, R., Aubourg, É., Balland, C., Bareyre, P., Beaulieu, J. P., Charlot, X., Conley, A., Coutures, C., Dahlén, T., Derue, F., Fan, X., Ferlet, R., Folatelli, G., Fouqué, P., Garavini, G., Glicenstein, J. F., Goldman, B., Goobar, A., Gould, A., Graff, D., Gros, M., Haissinski, J., Hamadache, C., Hardin, D., Hook, I. M., de Kat, J., Kent, S., Kim, A., Lasserre, T., Le Guillou, L., Lesquoy, É., Loup, C., Magneville, C., Marquette, J. B., Maurice, É., Maury, A., Milsztajn, A., Moniez, M., Mouchet, M., Newberg, H., Nobili, S., Palanque-Delabrouille, N., Perdereau, O., Prévot, L., Rahal, Y. R., Regnault, N., Rich, J., Ruiz-Lapuente, P., Spiro, M., Tisserand, P., Vidal-Madjar, A., Vigroux, L., Walton, N. A., & Zylberajch, S. 2004, A&A, 423, 881

Blanton, M. R., Hogg, D. W., Bahcall, N. A., Brinkmann, J., Britton, M., Connolly, A. J., Csabai, I., Fukugita, M., Loveday, J., Meiksin, A., Munn, J. A., Nichol, R. C., Okamura, S., Quinn, T., Schneider, D. P., Shimasaku, K., Strauss, M. A., Tegmark, M., Vogeley, M. S., & Weinberg, D. H. 2003, ApJ, 592, 819

Blondin, S. & Tonry, J. L. 2007, ApJ, 666, 1024

Branch, D., Livio, M., Yungelson, L. R., Boffi, F. R., & Baron, E. 1995, PASP, 107, 1019

Cappellaro, E., Botticella, M. T., & Greggio, L. 2007, astro-ph/0706.1299

Cappellaro, E., Evans, R., & Turatto, M. 1999, A&A, 351, 459

Cardelli, J. A., Clayton, G. C., & Mathis, J. S. 1989, ApJ, 345, 245

Dahlen, T., Strolger, L.-G., Riess, A. G., Mobasher, B., Chary, R.-R., Conselice, C. J., Ferguson, H. C., Fruchter, A. S., Giavalisco, M., Livio, M., Madau, P., Panagia, N., & Tonry, J. L. 2004, ApJ, 613, 189

Förster, F., Wolf, C., Podsiadlowski, P., & Han, Z. 2006, MNRAS, 368, 1893

Frieman, J. A., Bassett, B., Becker, A., Choi, C., Cinabro, D., DeJongh, F., Depoy, D. L., Dilday, B., Doi, M., Garnavich, P. M., Hogan, C. J., Holtzman, J., Im, M., Jha, S., Kessler, R., Konishi, K., Lampeitl, H., Marriner, J., Marshall, J. L., McGinnis, D., Miknaitis, G., Nichol, R. C., Prieto, J. L., Riess, A. G., Richmond, M. W., Romani, R., Sako, M., Schneider, D. P., Smith, M., Takanashi, N., Tokita, K., van der Heyden, K., Yasuda, N., Zheng, C., Adelman-McCarthy, J., Annis, J., Assef, R. J., Barentine, J., Bender, R., Blandford, R. D., Boroski, W. N., Bremer, M., Brewington, H., Collins, C. A., Crotts, A., Dembicky, J., Eastman, J., Edge, A., Edmondson, E., Elson, E., Eyler, M. E., Filippenko, A. V., Foley, R. J., Frank, S., Goobar, A., Gueth, T., Gunn, J. E., Harvanek, M., Hopp, U., Ihara, Y., Ivezić, Ž., Kahn, S., Kaplan, J., Kent, S., Ketzeback, W., Kleinman, S. J., Kollatschny, W., Kron, R. G., Krzesiński, J., Lamenti, D., Leloudas, G., Lin, H., Long, D. C., Lucey, J., Lupton, R. H., Malanushenko, E., Malanushenko, V., McMillan, R. J., Mendez, J., Morgan, C. W., Morokuma, T., Nitta, A., Ostman, L., Pan, K., Rockosi, C. M., Romer, A. K., Ruiz-Lapuente, P., Saurage, G., Schlesinger, K., Snedden, S. A., Sollerman, J., Stoughton, C., Stritzinger, M., Subba Rao, M., Tucker, D., Vaisanen, P., Watson, L. C., Watters, S., Wheeler, J. C., Yanny, B., & York, D. 2008, AJ, 135, 338

Fukugita, M., Ichikawa, T., Gunn, J. E., Doi, M., Shimasaku, K., & Schneider, D. P. 1996, AJ, 111, 1748

Greggio, L. 2005, A&A, 441, 1055

Gunn, J. E., Carr, M., Rockosi, C., Sekiguchi, M., Berry, K., Elms, B., de Haas, E., Ivezić, Ž., Knapp, G., Lupton, R., Pauls, G., Simcoe, R., Hirsch, R., Sanford, D., Wang, S., York, D., Harris, F., Annis, J., Bartozek, L., Boroski, W., Bakken, J., Haldeman, M., Kent, S., Holm, S., Holmgren, D., Petravick, D., Prosapio, A., Rechenmacher, R., Doi, M., Fukugita, M., Shimasaku, K., Okada, N., Hull, C., Siegmund, W., Mannery, E., Blouke, M., Heidtman, D., Schneider, D., Lucinio, R., & Brinkman, J. 1998, AJ, 116, 3040

Gunn, J. E., Siegmund, W. A., Mannery, E. J., Owen, R. E., Hull, C. L., Leger, R. F., Carey, L. N., Knapp, G. R., York, D. G., Boroski, W. N., Kent, S. M., Lupton, R. H., Rockosi, C. M., Evans, M. L., Waddell, P., Anderson, J. E., Annis, J., Barentine, J. C., Bartoszek, L. M., Bastian, S., Bracker, S. B., Brewington, H. J., Briegel, C. I., Brinkmann, J., Brown, Y. J., Carr, M. A., Czarapata, P. C., Drennan, C. C., Dombeck, T., Federwitz, G. R., Gillespie, B. A., Gonzales, C., Hansen, S. U., Harvanek, M., Hayes, J., Jordan, W., Kinney, E., Klaene, M., Kleinman, S. J., Kron, R. G., Kresinski, J., Lee, G., Limmongkol, S., Lindenmeyer, C. W., Long, D. C., Loomis, C. L., McGehee, P. M., Mantsch, P. M., Neilsen, Jr., E. H., Neswold, R. M., Newman, P. R., Nitta, A., Peoples, J. J., Pier, J. R., Prieto, P. S., Prosapio, A., Rivetta, C., Schneider, D. P., Snedden, S., & Wang, S.-i. 2006, AJ, 131, 2332

Hamuy, M., Phillips, M., Suntzeff, N., & Maza, J. 2003, IAU Circ., 8151, 2

Hamuy, M., Phillips, M. M., Suntzeff, N. B., Schommer, R. A., Maza, J., & Aviles, R. 1996, AJ, 112, 2391

Hardin, D., Afonso, C., Alard, C., Albert, J. N., Amadon, A., Andersen, J., Ansari, R., Aubourg, É., Bareyre, P., Bauer, F., Beaulieu, J. P., Blanc, G., Bouquet, A., Char, S., Charlot, X., Couchot, F., Coutures, C., Derue, F., Ferlet, R., Glicenstein, J. F., Goldman, B., Gould, A., Graff, D., Gros, M., Haissinski, J., Hamilton, J. C., de Kat, J., Kim, A., Lasserre, T., Lesquoy, É., Loup, C., Magneville, C., Mansoux, B., Marquette, J. B., Maurice, É., Milsztajn, A., Moniez, M., Palanque-Delabrouille, N., Perdereau, O., Prévot, L., Regnault, N., Rich, J., Spiro, M., Vidal-Madjar, A., Vigroux, L., Zylberajch, S., & The EROS Collaboration. 2000, A&A, 362, 419

Höflich, P., Khokhlov, A., Wheeler, J. C., Phillips, M. M., Suntzeff, N. B., & Hamuy, M. 1996, ApJ, 472, L81+

Höflich, P., Khokhlov, A. M., & Wheeler, J. C. 1995, ApJ, 444, 831

Hogg, D. W., Finkbeiner, D. P., Schlegel, D. J., & Gunn, J. E. 2001, AJ, 122, 2129

Holtzman et al., J. 2008, submitted to AJ

Hopkins, A. M. & Beacom, J. F. 2006, ApJ, 651, 142

Howell, D. A., Sullivan, M., Conley, A., & Carlberg, R. 2007, astro-ph/0701912

Ivezić, Ž., Lupton, R. H., Schlegel, D., Boroski, B., Adelman-McCarthy, J., Yanny, B., Kent, S., Stoughton, C., Finkbeiner, D., Padmanabhan, N., Rockosi, C. M., Gunn, J. E., Knapp, G. R., Strauss, M. A., Richards, G. T., Eisenstein, D., Nicinski, T., Kleinman,

S. J., Krzesinski, J., Newman, P. R., Snedden, S., Thakar, A. R., Szalay, A., Munn, J. A., Smith, J. A., Tucker, D., & Lee, B. C. 2004, Astronomische Nachrichten, 325, 583

Ivezić, Ž., Smith, J. A., Miknaitis, G., Lin, H., Tucker, D., Lupton, R. H., Gunn, J. E., Knapp, G. R., Strauss, M. A., Sesar, B., Doi, M., Tanaka, M., Fukugita, M., Holtzman, J., Kent, S., Yanny, B., Schlegel, D., Finkbeiner, D., Padmanabhan, N., Rockosi, C. M., Jurić, M., Bond, N., Lee, B., Stoughton, C., Jester, S., Harris, H., Harding, P., Morrison, H., Brinkmann, J., Schneider, D. P., & York, D. 2007, AJ, 134, 973

James, F. & Roos, M. 1994, MINUIT, CERN, Geneva

Jha, S., Riess, A. G., & Kirshner, R. P. 2007, ApJ, 659, 122

Kasen, D. & Woosley, S. E. 2007, ApJ, 656, 661

Kuznetsova, N., Barbary, K., Connolly, B., Kim, A. G., Pain, R., Roe, N. A., Aldering, G., Amanullah, R., Dawson, K., Doi, M., Fadeyev, V., Fruchter, A. S., Gibbons, R., Goldhaber, G., Goobar, A., Gude, A., Knop, R. A., Kowalski, M., Lidman, C., Morokuma, T., Meyers, J., Perlmutter, S., Rubin, D., Schlegel, D. J., Spadafora, A. L., Stanishev, V., Strovink, M., Suzuki, N., Wang, L., & Yasuda, N. 2007, ArXiv e-prints, 710

Li, W., Filippenko, A. V., Chornock, R., Berger, E., Berlind, P., Calkins, M. L., Challis, P., Fassnacht, C., Jha, S., Kirshner, R. P., Matheson, T., Sargent, W. L. W., Simcoe, R. A., Smith, G. H., & Squires, G. 2003, PASP, 115, 453

Lupton, R., Gunn, J. E., Ivezić, Z., Knapp, G. R., & Kent, S. 2001, in ASP Conf. Ser. 238: Astronomical Data Analysis Software and Systems X, ed. F. R. Harnden, Jr., F. A. Primini, & H. E. Payne, 269–+

Lupton, R. H., Gunn, J. E., & Szalay, A. S. 1999, AJ, 118, 1406

Madgwick, D. S., Hewett, P. C., Mortlock, D. J., & Wang, L. 2003, ApJ, 599, L33

Mannucci, F., Della Valle, M., & Panagia, N. 2006, MNRAS, 370, 773

Mannucci, F., Della Valle, M., Panagia, N., Cappellaro, E., Cresci, G., Maiolino, R., Petrosian, A., & Turatto, M. 2005, A&A, 433, 807

Matheson, T., Blondin, S., Foley, R. J., Chornock, R., Filippenko, A. V., Leibundgut, B., Smith, R. C., Sollerman, J., Spyromilio, J., Kirshner, R. P., Clocchiatti, A., Aguilera, C., Barris, B., Becker, A. C., Challis, P., Covarrubias, R., Garnavich, P., Hicken, M.,

Jha, S., Krisciunas, K., Li, W., Miceli, A., Miknaitis, G., Prieto, J. L., Rest, A., Riess, A. G., Salvo, M. E., Schmidt, B. P., Stubbs, C. W., Suntzeff, N. B., & Tonry, J. L. 2005, AJ, 129, 2352

Neill, J. D., Sullivan, M., Balam, D., Pritchet, C. J., Howell, D. A., Perrett, K., Astier, P., Aubourg, E., Basa, S., Carlberg, R. G., Conley, A., Fabbro, S., Fouchez, D., Guy, J., Hook, I., Pain, R., Palanque-Delabrouille, N., Regnault, N., Rich, J., Taillet, R., Aldering, G., Antilogus, P., Arsenijevic, V., Balland, C., Baumont, S., Bronder, J., Ellis, R. S., Filiol, M., Gonçalves, A. C., Hardin, D., Kowalski, M., Lidman, C., Lusset, V., Mouchet, M., Mourao, A., Perlmutter, S., Ripoche, P., Schlegel, D., & Tao, C. 2006, AJ, 132, 1126

Nugent, P., Kim, A., & Perlmutter, S. 2002, PASP, 114, 803

Nugent, P., Phillips, M., Baron, E., Branch, D., & Hauschildt, P. 1995, ApJ, 455, L147+

Oyaizu, H., Lima, M., Cunha, C. E., Lin, H., Frieman, J., & Sheldon, E. S. 2007, astro-ph/0708.0030

Pain, R., Fabbro, S., Sullivan, M., Ellis, R. S., Aldering, G., Astier, P., Deustua, S. E., Fruchter, A. S., Goldhaber, G., Goobar, A., Groom, D. E., Hardin, D., Hook, I. M., Howell, D. A., Irwin, M. J., Kim, A. G., Kim, M. Y., Knop, R. A., Lee, J. C., Lidman, C., McMahon, R. G., Nugent, P. E., Panagia, N., Pennypacker, C. R., Perlmutter, S., Ruiz-Lapuente, P., Schahmaneche, K., Schaefer, B., & Walton, N. A. 2002, ApJ, 577, 120

Phillips, M. M. 1993, ApJ, 413, L105

Phillips, M. M., Li, W., Frieman, J. A., Blinnikov, S. I., DePoy, D., Prieto, J. L., Milne, P., Contreras, C., Folatelli, G., Morrell, N., Hamuy, M., Suntzeff, N. B., Roth, M., González, S., Krzeminski, W., Filippenko, A. V., Freedman, W. L., Chornock, R., Jha, S., Madore, B. F., Persson, S. E., Burns, C. R., Wyatt, P., Murphy, D., Foley, R. J., Ganeshalingam, M., Serduke, F. J. D., Krisciunas, K., Bassett, B., Becker, A., Dilday, B., Eastman, J., Garnavich, P. M., Holtzman, J., Kessler, R., Lampeitl, H., Marriner, J., Frank, S., Marshall, J. L., Miknaitis, G., Sako, M., Schneider, D. P., van der Heyden, K., & Yasuda, N. 2007, PASP, 119, 360

Pier, J. R., Munn, J. A., Hindsley, R. B., Hennessy, G. S., Kent, S. M., Lupton, R. H., & Ivezić, Ž. 2003, AJ, 125, 1559

Poznanski, D., Maoz, D., Yasuda, N., Foley, R. J., Doi, M., Filippenko, A. V., Fukugita, M., Gal-Yam, A., Jannuzi, B. T., Morokuma, T., Oda, T., Schweiker, H., Sharon, K., Silverman, J. M., & Totani, T. 2007, MNRAS, 382, 1169

Prieto, J. L., Garnavich, P. M., Phillips, M. M., DePoy, D. L., Parrent, J., Pooley, D., Dwarkadas, V. V., Baron, E., Bassett, B., Becker, A., Cinabro, D., DeJongh, F., Dilday, B., Doi, M., Frieman, J. A., Hogan, C. J., Holtzman, J., Jha, S., Kessler, R., Konishi, K., Lampeitl, H., Marriner, J., Marshall, J. L., Miknaitis, G., Nichol, R. C., Riess, A. G., Richmond, M. W., Romani, R., Sako, M., Schneider, D. P., Smith, M., Takanashi, N., Tokita, K., van der Heyden, K., Yasuda, N., Zheng, C., Wheeler, J. C., Barentine, J., Dembicky, J., Eastman, J., Frank, S., Ketzeback, W., McMillan, R. J., Morrell, N., Folatelli, G., Contreras, C., Burns, C. R., Freedman, W. L., Gonzalez, S., Hamuy, M., Krzeminski, W., Madore, B. F., Murphy, D., Persson, S. E., Roth, M., & Suntzeff, N. B. 2007, astro-ph/0706.4088

Pskovskii, I. P. 1977, Soviet Astronomy, 21, 675

Quimby, R., Höflich, P., Kannappan, S. J., Odewahn, S. C., & Terrazas, E. 2005, Central Bureau Electronic Telegrams, 266, 1

Riess, A. G., Press, W. H., & Kirshner, R. P. 1996, ApJ, 473, 88

Sako, M., Bassett, B., Becker, A., Cinabro, D., DeJongh, F., Depoy, D. L., Dilday, B., Doi, M., Frieman, J. A., Garnavich, P. M., Hogan, C. J., Holtzman, J., Jha, S., Kessler, R., Konishi, K., Lampeitl, H., Marriner, J., Miknaitis, G., Nichol, R. C., Prieto, J. L., Riess, A. G., Richmond, M. W., Romani, R., Schneider, D. P., Smith, M., Subba Rao, M., Takanashi, N., Tokita, K., van der Heyden, K., Yasuda, N., Zheng, C., Barentine, J., Brewington, H., Choi, C., Dembicky, J., Harnavek, M., Ihara, Y., Im, M., Ketzeback, W., Kleinman, S. J., Krzesiński, J., Long, D. C., Malanushenko, E., Malanushenko, V., McMillan, R. J., Morokuma, T., Nitta, A., Pan, K., Saurage, G., & Snedden, S. A. 2008, AJ, 135, 348

Scannapieco, E. & Bildsten, L. 2005, ApJ, 629, L85

Schechter, P. L., Mateo, M., & Saha, A. 1993, PASP, 105, 1342

Schlegel, D. J., Finkbeiner, D. P., & Davis, M. 1998, ApJ, 500, 525

Shimasaku, K., Fukugita, M., Doi, M., Hamabe, M., Ichikawa, T., Okamura, S., Sekiguchi, M., Yasuda, N., Brinkmann, J., Csabai, I., Ichikawa, S.-I., Ivezić, Z., Kunszt, P. Z., Schneider, D. P., Szokoly, G. P., Watanabe, M., & York, D. G. 2001, AJ, 122, 1238

Smith, J. A., Tucker, D. L., Kent, S., Richmond, M. W., Fukugita, M., Ichikawa, T., Ichikawa, S.-i., Jorgensen, A. M., Uomoto, A., Gunn, J. E., Hamabe, M., Watanabe, M., Tolea, A., Henden, A., Annis, J., Pier, J. R., McKay, T. A., Brinkmann, J., Chen, B., Holtzman, J., Shimasaku, K., & York, D. G. 2002, AJ, 123, 2121

Stoughton, C., Lupton, R. H., Bernardi, M., Blanton, M. R., Burles, S., Castander, F. J., Connolly, A. J., Eisenstein, D. J., Frieman, J. A., Hennessy, G. S., Hindsley, R. B., Ivezić, Ž., Kent, S., Kunszt, P. Z., Lee, B. C., Meiksin, A., Munn, J. A., Newberg, H. J., Nichol, R. C., Nicinski, T., Pier, J. R., Richards, G. T., Richmond, M. W., Schlegel, D. J., Smith, J. A., Strauss, M. A., SubbaRao, M., Szalay, A. S., Thakar, A. R., Tucker, D. L., Vanden Berk, D. E., Yanny, B., Adelman, J. K., Anderson, Jr., J. E., Anderson, S. F., Annis, J., Bahcall, N. A., Bakken, J. A., Bartelmann, M., Bastian, S., Bauer, A., Berman, E., Böhringer, H., Boroski, W. N., Bracker, S., Briegel, C., Briggs, J. W., Brinkmann, J., Brunner, R., Carey, L., Carr, M. A., Chen, B., Christian, D., Colestock, P. L., Crocker, J. H., Csabai, I., Czarapata, P. C., Dalcanton, J., Davidsen, A. F., Davis, J. E., Dehnen, W., Dodelson, S., Doi, M., Dombeck, T., Donahue, M., Ellman, N., Elms, B. R., Evans, M. L., Eyer, L., Fan, X., Federwitz, G. R., Friedman, S., Fukugita, M., Gal, R., Gillespie, B., Glazebrook, K., Gray, J., Grebel, E. K., Greenawalt, B., Greene, G., Gunn, J. E., de Haas, E., Haiman, Z., Haldeman, M., Hall, P. B., Hamabe, M., Hansen, B., Harris, F. H., Harris, H., Harvanek, M., Hawley, S. L., Hayes, J. J. E., Heckman, T. M., Helmi, A., Henden, A., Hogan, C. J., Hogg, D. W., Holmgren, D. J., Holtzman, J., Huang, C.-H., Hull, C., Ichikawa, S.-I., Ichikawa, T., Johnston, D. E., Kauffmann, G., Kim, R. S. J., Kimball, T., Kinney, E., Klaene, M., Kleinman, S. J., Klypin, A., Knapp, G. R., Korienek, J., Krolik, J., Kron, R. G., Krzesiński, J., Lamb, D. Q., Leger, R. F., Limmongkol, S., Lindenmeyer, C., Long, D. C., Loomis, C., Loveday, J., MacKinnon, B., Mannery, E. J., Mantsch, P. M., Margon, B., McGehee, P., McKay, T. A., McLean, B., Menou, K., Merelli, A., Mo, H. J., Monet, D. G., Nakamura, O., Narayanan, V. K., Nash, T., Neilsen, Jr., E. H., Newman, P. R., Nitta, A., Odenkirchen, M., Okada, N., Okamura, S., Ostriker, J. P., Owen, R., Pauls, A. G., Peoples, J., Peterson, R. S., Petravick, D., Pope, A., Pordes, R., Postman, M., Prosapio, A., Quinn, T. R., Rechenmacher, R., Rivetta, C. H., Rix, H.-W., Rockosi, C. M., Rosner, R., Ruthmansdorfer, K., Sandford, D., Schneider, D. P., Scranton, R., Sekiguchi, M., Sergey, G., Sheth, R., Shimasaku, K., Smee, S., Snedden, S. A., Stebbins, A., Stubbs, C., Szapudi, I., Szkody, P., Szokoly, G. P., Tabachnik, S., Tsvetanov, Z., Uomoto, A., Vogeley, M. S., Voges, W., Waddell, P., Walterbos, R., Wang, S.-i., Watanabe, M., Weinberg, D. H., White, R. L., White, S. D. M., Wilhite, B., Wolfe, D., Yasuda, N., York, D. G., Zehavi, I., & Zheng, W. 2002, AJ, 123, 485

Strateva, I., Ivezić, Ž., Knapp, G. R., Narayanan, V. K., Strauss, M. A., Gunn, J. E., Lupton, R. H., Schlegel, D., Bahcall, N. A., Brinkmann, J., Brunner, R. J., Budavári, T., Csabai, I., Castander, F. J., Doi, M., Fukugita, M., Győry, Z., Hamabe, M., Hennessy, G., Ichikawa, T., Kunszt, P. Z., Lamb, D. Q., McKay, T. A., Okamura, S., Racusin, J., Sekiguchi, M., Schneider, D. P., Shimasaku, K., & York, D. 2001, AJ, 122, 1861

Strolger, L.-G. & Riess, A. G. 2006, AJ, 131, 1629

Strolger, L.-G., Riess, A. G., Dahlen, T., Livio, M., Panagia, N., Challis, P., Tonry, J. L., Filippenko, A. V., Chornock, R., Ferguson, H., Koekemoer, A., Mobasher, B., Dickinson, M., Giavalisco, M., Casertano, S., Hook, R., Blondin, S., Leibundgut, B., Nonino, M., Rosati, P., Spinrad, H., Steidel, C. C., Stern, D., Garnavich, P. M., Matheson, T., Grogin, N., Hornschemeier, A., Kretchmer, C., Laidler, V. G., Lee, K., Lucas, R., de Mello, D., Moustakas, L. A., Ravindranath, S., Richardson, M., & Taylor, E. 2004, ApJ, 613, 200

Sullivan, M., Le Borgne, D., Pritchet, C. J., Hodsman, A., Neill, J. D., Howell, D. A., Carlberg, R. G., Astier, P., Aubourg, E., Balam, D., Basa, S., Conley, A., Fabbro, S., Fouchez, D., Guy, J., Hook, I., Pain, R., Palanque-Delabrouille, N., Perrett, K., Regnault, N., Rich, J., Taillet, R., Baumont, S., Bronder, J., Ellis, R. S., Filiol, M., Lusset, V., Perlmutter, S., Ripoche, P., & Tao, C. 2006, ApJ, 648, 868

Tonry, J. & Davis, M. 1979, AJ, 84, 1511

Tonry, J. L., Schmidt, B. P., Barris, B., Candia, P., Challis, P., Clocchiatti, A., Coil, A. L., Filippenko, A. V., Garnavich, P., Hogan, C., Holland, S. T., Jha, S., Kirshner, R. P., Krisciunas, K., Leibundgut, B., Li, W., Matheson, T., Phillips, M. M., Riess, A. G., Schommer, R., Smith, R. C., Sollerman, J., Spyromilio, J., Stubbs, C. W., & Suntzeff, N. B. 2003, ApJ, 594, 1

Tucker, D. L., Kent, S., Richmond, M. W., Annis, J., Smith, J. A., Allam, S. S., Rodgers, C. T., Stute, J. L., Adelman-McCarthy, J. K., Brinkmann, J., Doi, M., Finkbeiner, D., Fukugita, M., Goldston, J., Greenway, B., Gunn, J. E., Hendry, J. S., Hogg, D. W., Ichikawa, S.-I., Ivezić, Ž., Knapp, G. R., Lampeitl, H., Lee, B. C., Lin, H., McKay, T. A., Merrelli, A., Munn, J. A., Neilsen, Jr., E. H., Newberg, H. J., Richards, G. T., Schlegel, D. J., Stoughton, C., Uomoto, A., & Yanny, B. 2006, Astronomische Nachrichten, 327, 821

Yamauchi, C., Ichikawa, S.-i., Doi, M., Yasuda, N., Yagi, M., Fukugita, M., Okamura, S., Nakamura, O., Sekiguchi, M., & Goto, T. 2005, AJ, 130, 1545

York, D. G., Adelman, J., Anderson, Jr., J. E., Anderson, S. F., Annis, J., Bahcall, N. A., Bakken, J. A., Barkhouser, R., Bastian, S., Berman, E., Boroski, W. N., Bracker, S., Briegel, C., Briggs, J. W., Brinkmann, J., Brunner, R., Burles, S., Carey, L., Carr, M. A., Castander, F. J., Chen, B., Colestock, P. L., Connolly, A. J., Crocker, J. H., Csabai, I., Czarapata, P. C., Davis, J. E., Doi, M., Dombeck, T., Eisenstein, D., Ellman, N., Elms, B. R., Evans, M. L., Fan, X., Federwitz, G. R., Fiscelli, L., Friedman, S., Frieman, J. A., Fukugita, M., Gillespie, B., Gunn, J. E., Gurbani, V. K., de Haas, E., Haldeman, M., Harris, F. H., Hayes, J., Heckman, T. M., Hennessy, G. S., Hindsley, R. B., Holm, S., Holmgren, D. J., Huang, C.-h., Hull, C., Husby, D., Ichikawa, S.-I., Ichikawa, T., Ivezić, Ž., Kent, S., Kim, R. S. J., Kinney, E., Klaene, M., Kleinman, A. N., Kleinman, S., Knapp, G. R., Korienek, J., Kron, R. G., Kunszt, P. Z., Lamb, D. Q., Lee, B., Leger, R. F., Limmongkol, S., Lindenmeyer, C., Long, D. C., Loomis, C., Loveday, J., Lucinio, R., Lupton, R. H., MacKinnon, B., Mannery, E. J., Mantsch, P. M., Margon, B., McGehee, P., McKay, T. A., Meiksin, A., Merelli, A., Monet, D. G., Munn, J. A., Narayanan, V. K., Nash, T., Neilsen, E., Neswold, R., Newberg, H. J., Nichol, R. C., Nicinski, T., Nonino, M., Okada, N., Okamura, S., Ostriker, J. P., Owen, R., Pauls, A. G., Peoples, J., Peterson, R. L., Petravick, D., Pier, J. R., Pope, A., Pordes, R., Prosapio, A., Rechenmacher, R., Quinn, T. R., Richards, G. T., Richmond, M. W., Rivetta, C. H., Rockosi, C. M., Ruthmansdorfer, K., Sandford, D., Schlegel, D. J., Schneider, D. P., Sekiguchi, M., Sergey, G., Shimasaku, K., Siegmund, W. A., Smee, S., Smith, J. A., Snedden, S., Stone, R., Stoughton, C., Strauss, M. A., Stubbs, C., SubbaRao, M., Szalay, A. S., Szapudi, I., Szokoly, G. P., Thakar, A. R., Tremonti, C., Tucker, D. L., Uomoto, A., Vanden Berk, D., Vogeley, M. S., Waddell, P., Wang, S.-i., Watanabe, M., Weinberg, D. H., Yanny, B., & Yasuda, N. 2000, AJ, 120, 1579

Zheng et al., C. 2008, submitted to AJ